# International Journal of Engineering Sciences & Research Technology

(A Peer Reviewed Online Journal)
Impact Factor: 5.164

IJESRT

RESEARCHERID
THOMSON REUTERS

[Ekott *et al.*, 12(7): July, 2023]
IC™ Value: 3.00

ISSN: 2277-9655
Impact Factor: 5.164
CODEN: IJESS7

IJESRT

INTERNATIONAL JOURNAL OF ENGINEERING SCIENCES & RESEARCH TECHNOLOGY

# BRIGHT RED LUMINESCENCE EMISSION FROM $PR^{3+}$ - $MN^{2+}$ PAIR OF IONS DOPED IN CAO-PBO-$B_2O_3$-$SIO_2$ GLASS WEB FOR RED LIGHT SENSORS AND LED APPLICATIONS

**K. Kalyan Chakravarthi and M. Rami Reddy***
Department of Physics, Acharya Nagarjuna University, Nagarjuna Nagar-522503, India.

**DOI**: 10.5281/zenodo.8182475

## ABSTRACT

The novel synthesis remote composition of CaO-PbO-$B_2O_3$-$SiO_2$: $Pr^{3+}$-$Mn^{2+}$ glasses were prepared by melt-quenching technique. The absorption spectra of $Pr^{3+}$-$Mn^{2+}$ co-doped ions glasses exhibits various optical transitions in Uv-vis-NIR region. The photoluminescence spectra of $Pr^{3+}$- $Mn^{2+}$ pair of ions contain glasses exhibited in various luminescent transitions. Among all luminescent transitions, the high intense $^3P_0 \rightarrow {}^3H_6$ (696 nm) was observed that fall on bright red region due to its high crystal field strength of octahedral $Mn^{2+}$ sensitizer ions. The all optical absorption and luminescent transitions of $Pr^{3+}$ activator ions are related to $4f^2$ intraconfigurational transitions. Among all prepared samples, the PrMn1.0 glass shows high luminescent energy transfer of metal ($Mn^{2+}$) to metal ($Pr^{3+}$) intervalence charge transfer transition of $d^5 \rightarrow f^2$. The EPR spectra exhibited sextet signal due to presence of octahedral $Mn^{2+}$ paramagnetic ions. The $g \approx 2.02$ shows at centre of spectrogram were identified as $Mn^{2+}$ ($O_h$) ions. From the quantitative analysis of these results, the energy transfer transition is associated from $Mn^{2+}$ donor ions to $Pr^{3+}$ activator ions ($Mn^{2+} \rightarrow Pr^{3+}$). The IR spectra confirmed the presence of borosilicate molecular dynamic units. XRD analysis suggest that all glass samples are inorganic non-crystalline structure without narrow sharp peaks.

**Keywords**: Lead borosilicate glasses, optical absorption, Photoluminescence, Energy transfer ($d^5 \rightarrow f^2$) EPR, FTIR

## 1. INTRODUCTION

Oxide glasses are the best host webs for wide novel potential applications due to its high transparent, strong glass forming ability and remote composition. Oxide glasses are luminescent key host for tuneable Solid State Visible Lasers (SSVL) and good lasing properties in various field of applications. Nowadays ever-changing advanced laser technical applications are in various fields. Due to high-temperature resistance, borosilicate is also very stable and can be used for optical devices. The borosilicate glass is commonly used for studio spotlights and HID lamps. A recent study has involved altering the chemical compositions of a borosilicate glass made of solid state display. The altered chemical composition of borosilicate also be used to manufacture LEDs. Space applications include reflecting telescopes for its resistance to thermal shock. This allows for precise mirror surfaces that won't distort under extreme temperature variations. Hale Telescope's has 200 inch mirror that is made of borosilicate glass. Borosilicate glass can be moulded into high precision optical components such as tuneable laser, lenses in telescopes and other precision optical devices. The Borosilicate glass has good optical and luminescence properties with ability to transmit light through the visible range of the spectrum and in the near ultra-violet range widely used in the field of spectroscopy. Borosilicate glasses are used for optical lenses with low dispersion and high refractive index [1].

Glass is defined as a high molecular weight compound formed by the combination of number of glass formers, intermediates, glass modifiers and small amount of Transition, Rare earth ions. Amorphous glasses are isotropic in nature. Glasses were pseudo material or super cooled liquids. Synthetic glass systems are man-made glasses in laboratory have wide range high potential applications. A large number of glass applications in different fields depend on their unique mechanical properties, physical properties, concentration of co-doped Transition

ISSN: 2277-9655
Impact Factor: 5.164
CODEN: IJESS7

metal ions and Rare earth ions. These mechanical properties and physical properties of the glasses are governed by intermolecular forces between glass formers, intermediates and glass modifiers. Glass fibres are the thread forming glass solids which possess high tensile strength and high modulus.

Borosilicate glasses have good optical cavity, wide range advanced technological applications in various different fields such as solar energy, optoelectronics and nuclear waste immobilization. The PbO (intermediate oxide) introduced into borosilicate titled glass host which results structural changes by strong influence of the local network due to its several properties such as low melting temperature, high density, high refractive index that improves the chemical durability and enhance the resistance against diversification. The variable oxidation phenomenon of Transition Metal ions are paramagnetic inducers and these are able to give strong EPR hyperfine splitting structure in resonance spectrogram. Manganese ions exist in different valence states with different coordination in glass matrices. The content of manganese in different coordination's in different valence exist in the glass depends upon the quantitative properties of glass formers, glass modifiers, size of the $Mn^{2+}$ ions in the glass structure their Crystal Field Strength (CFS), concentration of $Mn^{2+}$ ions and mobility of the modifier cation. Among the transition metal ions, $Mn^{2+}$ is a typical luminescent ion with good high potential applications. Another characteristic feature of the $Mn^{2+}$ emission in the long decay lifetime (microseconds to milliseconds) due to the spin-forbidden $^4T_1$ ($^4G$) $\rightarrow$ $^6A_1$ ($^6S$) transition of d-d transition. Glass host are co-doped with RE and TM ions determines the efficient luminescent laser visible colour. Due to unique advantages of glasses, $Mn^{2+}$ contain glass is a high-security level optical information storage. Manganese plays important liniment of active red centres in borosilicate glasses. Manganese exhibit luminescent color centres in oxide and non-oxide glass systems. Transition metal ions acts for reversible energy storage devices such as metal-air batteries, supercapacitors etc. Varying oxidation of Transition metal ions plays an important role for photo-energy conversion.

Manganese deployed based oxide glass are mostly owing to their remarkable diversity in glass structure, high theoretical energy density, low cost and environmental friendliness. The oxidation of $Mn^{2+}$ in the electrolyte during charge, which contribute charge transfer to the acceptor. The addition of small mol% of MnO to borosilicate glass host facilitates the enhancement in mechanical properties, physical properties, optical, magnetic and luminescence properties of the glasses.

The isolated $Pr^{3+}$ ions contain oxide glasses have extensive novel technical applications as UV-vis-NIR wavelength region such as optical amplifiers up-converters, optical fibres and laser due to its ample numerous energy states. The electronic transition between the ground to excited state to lower states of the $4f^n$-intraconfigurational gives the optical and emission spectrums of the $Pr^{3+}$ (rare earth) ions. Borosilicate system glass which on heating undergo extensive cross-linking in moulds and again become infusible. Borosilicate host glass were excellent opportunity for luminescent red visible colour applicable in SSD, optical devices. Due to the high viscosity phenomena of borosilicate glasses are used as optical wave guide systems in communication purpose. Glass webs have unique advantages in electron and metal ions centres trapping in optical storage for its transparent ability. Borosilicate glass is suitable host for RE and TM ions improves the optical performance. Among 3d transition series and period, Manganese transition metal mostly stabilized in divalent (2-fold) valence state.

## 2. SYNTHESIS REACTION OF GLASSES

The high stable, high quality, high viscosity and strong homogeneity of the glass system, the chemical reagents such as $B_2O_3$+$SiO_2$, PbO, CaO, $Pr_2O_3$ and MnO are participated in the chemical combination reaction to form novel glass composition are depicts in Figure 1.

## 3. EXPERIMENTAL PROCEDURE

Commercial Glasses of composition are 20 CaO - (29-x) PbO – 25 $B_2O_3$ - 25 $SiO_2$ : 1$Pr_2O_3$ + x MnO (where 'x' varies from 0 to 1 mol % with a step of 0.2 mol %) were prepared by conventional melt-quenching technique. The high purity AR-grade (99.9%) commercial chemicals CaO, PbO, $B_2O_3$, $SiO_2$, $Pr_2O_3$ and MnO are oxide powder materials in the appropriate amounts of chemicals are weighed and powders are mixed in the composition ratios. Agate mortar and pestle grinded to obtain homogeneous mixture for de-carbonation. The well mixed powder placed in procelain crucible heated in an electric furnace at 490 $^oC$ for 35 minutes eliminate the carbonate and water vapour residuals. After de-carbonation of the glass powder is removed from furnace

ISSN: 2277-9655
Impact Factor: 5.164
CODEN: IJESS7

again agate mortar and pestle grinded to obtain homogeneous glass mixture for melt quenching process. A 50 ml SiC crucible is used to melt finely mixed powders of chemicals with the use of a programmable furnace. The melting point of glasses were estimated to be at 978 °C. Final transparent bubble-free melt discharged on pre-heated brass plate and pressed quickly with another brass plate to get uniform thickness. These glass samples instantly transferred to another furnace previously kept at 360 °C. Annealing was done in the muffle furnace at 360 °C for 6 hours to remove internal stresses of all the prepared glasses. Finally the $Pr^{3+}$ - $Mn^{2+}$ ions co-doped CaO - PbO - $B_2O_3$ - $SiO_2$ glass samples were polished with different grades of emery powder in required shapes for UV-visible-NIR and other spectroscopic measurements. The glass compositions used for the present Investigation are given in Table 1.

***Table 1: Glass Composition of CaO-PbO-$B_2O_3$-$SiO_2$: $Pr^{3+}$ - $Mn^{2+}$ ions co-doped glasses***

| S. No | Glass Codes | CaO | PbO | $B_2O_3$ | $SiO_2$ | $Pr_2O_3$ | MnO |
|---|---|---|---|---|---|---|---|
| | | mol % | mol % | mol % | mol % | mol % | mol % |
| 1 | Pr | 20 | 29 | 25 | 25 | 1 | - |
| 2 | PrMn0.2 | 20 | 28.8 | 25 | 25 | 1 | 0.2 |
| 3 | PrMn0.4 | 20 | 28.6 | 25 | 25 | 1 | 0.4 |
| 4 | PrMn0.6 | 20 | 28.4 | 25 | 25 | 1 | 0.6 |
| 5 | PrMn0.8 | 20 | 28.2 | 25 | 25 | 1 | 0.8 |
| 6 | PrMn1.0 | 20 | 28 | 25 | 25 | 1 | 1.0 |

Hereafter the host glass coded as CaPbBSi and other glasses coded as Pr, PrMn0.2, PrMn0.4, PrMn0.6, PrMn0.8, PrMn1.0 glass systems are prepared at melting temperature as 969, 970, 970, 976, 976 and 978 °C respectively. Figure.2 shows the prepared glossy glass samples with different compositions of transparent CaO-PbO-$B_2O_3$-$SiO_2$ : $Pr^{3+}$ - $Mn^{4+}$ ions co-doped glasses. The color of the glass samples changes from light blue to thick blue with increasing concentration of MnO content.

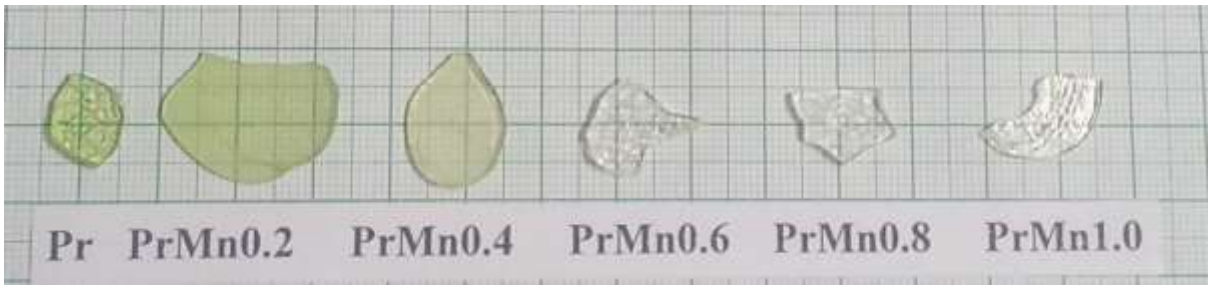


***Figure 2. CaO-PbO-$B_2O_3$-$SiO_2$: $Pr^{3+}$ - $Mn^{2+}$ ions co-doped glass samples***

**3.1 Sample Characterization**

The mass of the samples are recorded using a scale tech weighing balance. Scale Tech digital weighing balance with a precision of $10^{-4}$ gm/cm$^3$ recorded the weight of the glasses. The weights of the glasses were used to obtain the density values using Archimedes' technique. The Refractive index of these glass samples were measured by using Abbe's Refractometer. The X-ray diffraction patterns of the samples were recorded using a Shimadzu XRD-7000. The Optical absorption (UV-Vis-NIR) spectra were recorded JASCO, V-570 spectrophotometer from 200 to 2500 nm with an accuracy of 0.1 nm. The ESR spectra of powder samples were recorded at a room temperature using E11Z Varian X band (t=9.5GHz) of ESR spectrometer of 100 kHz field modulation. FTIR spectra were recorded on a JASCO-FTIR-140 spectrophotometer with resolution of 0.2 cm$^{-1}$. The spectral range 400-4000 cm$^{-1}$ using KBr pellets (300 mg) containing the pulverized sample (1.5 mg) and the spectra was analyzed in the range of 400-2000 cm$^{-1}$. The photoluminescence spectra was recorded at room temperature on a Photon Technology International (PTI) spectroflurometer with excited wavelength ($\lambda_{excitation}$) 487 nm from 300 to 900 nm.

ISSN: 2277-9655
Impact Factor: 5.164
CODEN: IJESS7

## 4. RESULTS

### 4.1 Physical Properties

The various physical properties of all prepared glass samples were calculated are shown in Table 2. The calculated values of physical properties of glass samples exhibits relevant variation related to physical property.

***Table 2: Various Physical properties of CaO-PbO-$B_2O_3$-$SiO_2$ : $Pr^{3+}$ - $Mn^{2+}$ ions co-doped glasses***

| Physical Properties | Pr | PrMn0.2 | PrMn0.4 | PrMn0.6 | PrMn0.8 | PrMn1.0 |
|---|---|---|---|---|---|---|
| Color of Glass Samples | Green | White | White | White | White | White |
| Thickness ***(t)*** (cm) | 0.1517 | 0.1014 | 0.1015 | 0.1014 | 0.1117 | 0.1015 |
| Density ***(d)*** (g/cm$^3$) (±0.004) | 4.8002 | 4.7916 | 4.7832 | 4.7743 | 4.7657 | 4.7571 |
| Average Molecular Weight ***(M)*** | 111.61 | 111.47 | 111.32 | 111.11 | 111.04 | 110.89 |
| Specific Volume ***($V_s$)*** (cm$^3$/gm) | 0.2083 | 0.2087 | 0.2091 | 0.2095 | 0.2098 | 0.2102 |
| Molar Volume ***($V_m$)*** (gm/cm$^3$) | 23.251 | 23.2636 | 23.273 | 23.2795 | 23.2998 | 23.3104 |
| Transition Metal Ion Concentration ***($N_i$)*** ($10^{22}$ ions/cm$^3$) (±0.005) | - - | 0.5178 | 1.0353 | 1.5529 | 2.0685 | 2.5839 |
| Electronic polarizability ***($\alpha_e$)*** ($10^{-23}$ ions/cm$^3$) (±0.005) | - - | 1.6455 | 0.8232 | 0.5488 | 0.4125 | 0.3327 |
| Interionic distance ***($R_i$)*** (Å) (±0.005) | - - | 5.7802 | 4.5884 | 4.0083 | 3.6432 | 3.3826 |
| Polaron radius ***($R_p$)*** (Å) (±0.005) | - - | 2.3294 | 1.8321 | 1.6153 | 1.4682 | 1.3632 |
| Field Strength ***($F_i$)*** ($10^{15}$ cm$^{-2}$) (±0.005) | - - | 5.5288 | 8.7741 | 11.4978 | 13.9172 | 16.1437 |
| Refractive Index ***($n_d$)*** (±0.0001) | 1.6641 | 1.6649 | 1.6652 | 1.6653 | 1.6684 | 1.6689 |
| Optical dielectric constant ***($\varepsilon_0$)*** (±0.005) | 1.7692 | 1.7719 | 1.7732 | 1.7762 | 1.7836 | 1.7853 |
| Reflection loss ***(R)*** | 0.2203 | 0.2207 | 0.2209 | 0.2209 | 0.2222 | 0.2225 |
| Molar reflectivity ***($R_M$)*** (cm$^{-3}$) (±0.005) | 8.2957 | 8.3031 | 8.3051 | 8.3174 | 8.3269 | 8.3324 |
| Oxygen Packing Density **(OPD)** | 80.914 | 80.836 | 80.749 | 80.527 | 80.461 | 80.373 |
| Optical Basicity **($\Lambda_{th}$)** | 0.5913 | 0.5987 | 0.6075 | 0.6156 | 0.6237 | 0.6311 |
| Dielectric constant **(ε)** | 2.7692 | 2.7719 | 2.7732 | 2.7762 | 2.7836 | 2.7853 |

### 4.2 X-Ray Diffraction Spectra

X-ray diffraction pattern is a non-destructive analytical technique that provides detailed information about the non-crystallographic structure, glass formation identification, phase identification and physical nature of glass composition. The X-ray diffraction patterns of $Pr^{3+}$- $Mn^{2+}$ ions co-doped CaO-PbO-$B_2O_3$-$SiO_2$ glasses are displayed in Figure 3. The diffraction peak position (2θ) depends on characteristics of wavelength (λ) used. The XRD analysis of all glass samples were recorded in the diffraction angle range of $10^o < 2\theta < 120^o$ at room temperature. The diffraction angles are taken up to an accuracy of ± $0.1^o$ lines drawn in the back ground of image only for better view of eye guiding.

ISSN: 2277-9655
Impact Factor: 5.164
CODEN: IJESS7

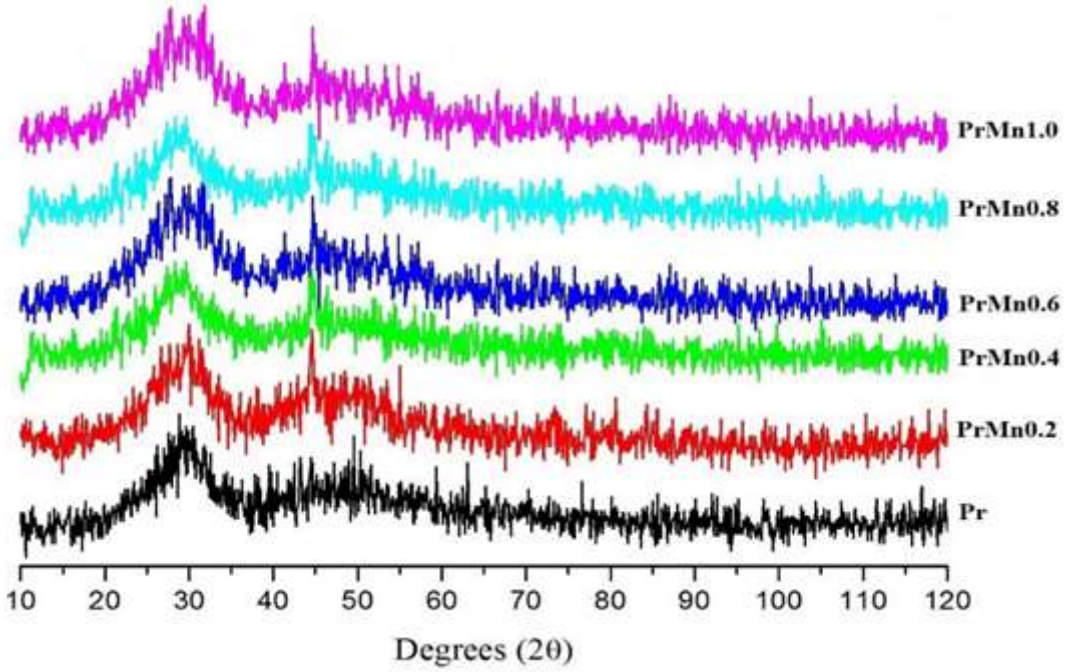


***Figure 3: X-Ray Diffraction pattern of CaO-PbO-$B_2O_3$-$SiO_2$: $Pr^{3+}$ - $Mn^{2+}$ ions co-doped glasses***

Two broad Braggs diffraction peaks are observed at lower angles around **~31º** and **~46º** (=2θ) without any sharp sticks. The direction and amount of peak shifted towards higher diffraction angle (2θ). The XRD analysis of phase glass composition is conformed highly disordered and glassy behavior of all the prepared glass samples.

**4.3 EDS Analysis**

The Energy Dispersive Spectroscopy of the chemical glass compositions were determined as displayed in Figure 4. The Figure.4 shows the Energy Dispersive Spectroscopy of the glass sample of 1 mol% of CaO-PbO-$B_2O_3$-$SiO_2$ : $Pr^{3+}$ - $Mn^{2+}$ ions co-doped glass.

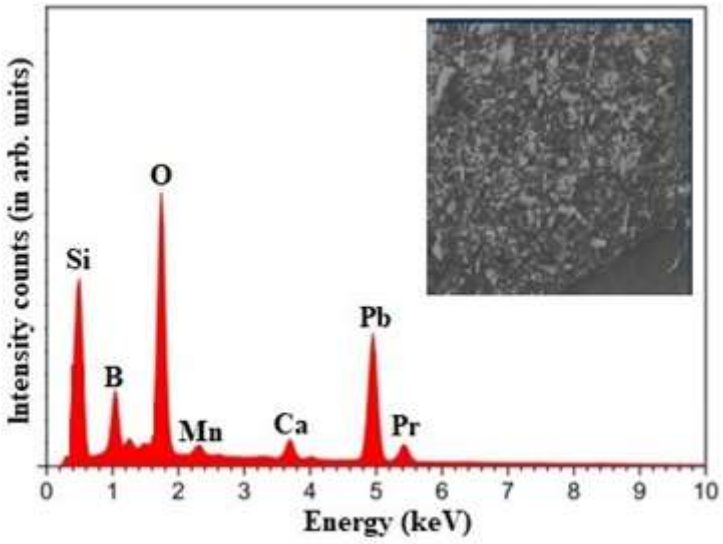


***Figure 4: EDS of CaO-PbO-$B_2O_3$-$SiO_2$: $Pr^{3+}$ - $Mn^{2+}$ ions co-doped glass***

ISSN: 2277-9655
Impact Factor: 5.164
CODEN: IJESS7

The EDS analysis confirms the presence of calcium (Ca), silicon (Si), boron (B), lead (Pb), oxygen (O), praseodymium (Pr) and manganese (Mn) elements in the glass network.

### 4.4 Differential Thermal Analysis

The thermal stability of glass is defined as the temperature range of the glass more precisely under cooled melt to draw into fiber. The spectrogram Figure.5 displays DTA curves for Pr, PrMn0.6 and PrMn1.0 glasses. From the spectrogram Figure.5 it was observed and recorded that the glass transition temperature ($T_g$), glass crystallization temperature ($T_c$) and glass melting temperature ($T_m$) of these glasses are given in Table 3.

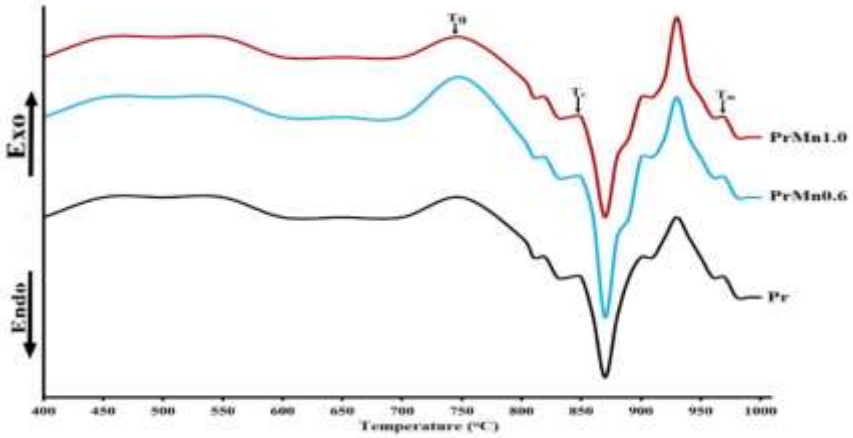


***Figure 5: Spectrogram DTA trace of CaO-PbO-$B_2O_3$-$SiO_2$: $Pr^{3+}$ - $Mn^{2+}$ ions co-doped glasses***

***Table 3: Values of glass transition temperature ($T_g$), crystallization temperature ($T_c$), melting temperature ($T_m$), Thermal Stability ($\Delta T$) and Hruby's Parameter (K) of various glass samples***

| Glass Sample Code | Glass Transition Temperature **($T_g$) ºC** | Glass Crystallization Temperature **($T_c$) ºC** | Glass Melting Temperature **($T_m$) ºC** | Thermal Stability **($\Delta T$) ºC** | Hruby's Parameter **(K)** |
|---|---|---|---|---|---|
| Pr | 741 | 839 | 976 | 98 | 0.7153 |
| PrMn0.6 | 744 | 841 | 981 | 97 | 0.6929 |
| PrMn1.0 | 747 | 843 | 986 | 96 | 0.6713 |

All the exothermic and endothermic thermograms variations are due to enthalpy change in 1.0 mol% MnO concentration was observed. The present glass samples of Pr, PrMn0.6, and PrMn1.0 are exhibited endothermic affect from 500ºC to 750ºC, glass transition temperature ($T_g$) is attributed. While at the high temperature, the exothermic change of hump due to its glass crystal growth ($T_c$) forming by melting of the glass with endothermic effect at glass melting temperature ($T_m$) are observed. The thermal stability factor $\Delta T=T_c-T_g$ is the difference between glass crystallization temperature ($T_c$) and glass transition temperature ($T_g$). The hump temperatures are assigned to the glass transition temperature ($T_g$), crystallization temperature ($T_c$) and melting temperature ($T_m$) respectively. From DTA Spectrogram analysis it was observed that $T_g$ depends on the strength of chemical bonds in the glass structure, bonding parameters between glass former and modifiers and glass remote composition. Hruby's Parameter (K) gives the information of the strong stability of the glass against devitrification. The stability of the glass in order of PrMn1.0 > PrMn0.6 > Pr. From the analyzed DTA spectrogram results reveals a glass with 1.0 mol% MnO concentration exhibiting highest thermal stability and from the Table.3 indicating PrMn1.0 is relatively highly stable glass forming ability against devitrification among all the glasses varying mol% of MnO content.

### 4.5 FTIR Spectra

The FTIR absorption spectra reviewed existence of glass forming local structural information, structural homogeneity, structural modifications and degree of structural compactness were analyzed in the glass chemical

ISSN: 2277-9655
Impact Factor: 5.164
CODEN: IJESS7

composition. The IR absorption is recorded at room temperature (37 $^{o}$C) with in wavenumber range of 4000-400 cm$^{-1}$. The FTIR spectra of $Pr^{3+}$- $Mn^{2+}$ pair of ions co-doped in CaO-PbO-$B_2O_3$-$SiO_2$ glasses shows strong, weak structural frequency modes of silicate, borate and borosilicate bonding functional structural information as shown in Figure.6

From the reviewed lead borosilicate glass literature survey, the structural frequency of borosilicate boning absorption bands are mainly exist in the following spectral series of bands, the first band at about $f_1$ (425 cm$^{-1}$), the second band $f_2$ (at 456 cm$^{-1}$), the third band $f_3$ (at 475 cm$^{-1}$), the fourth band centered $f_4$ (at 695 cm$^{-1}$), the fifth band $f_5$ (at 925 cm$^{-1}$) and the sixth band observed $f_6$ (at 1390 cm$^{-1}$). The summary data of the absorption band positons in the IR absorption spectra of $Pr^{3+}$- $Mn^{2+}$ pair of metal ions co-doped in CaO-PbO-$B_2O_3$-$SiO_2$ glasses are displaced in Table.4.

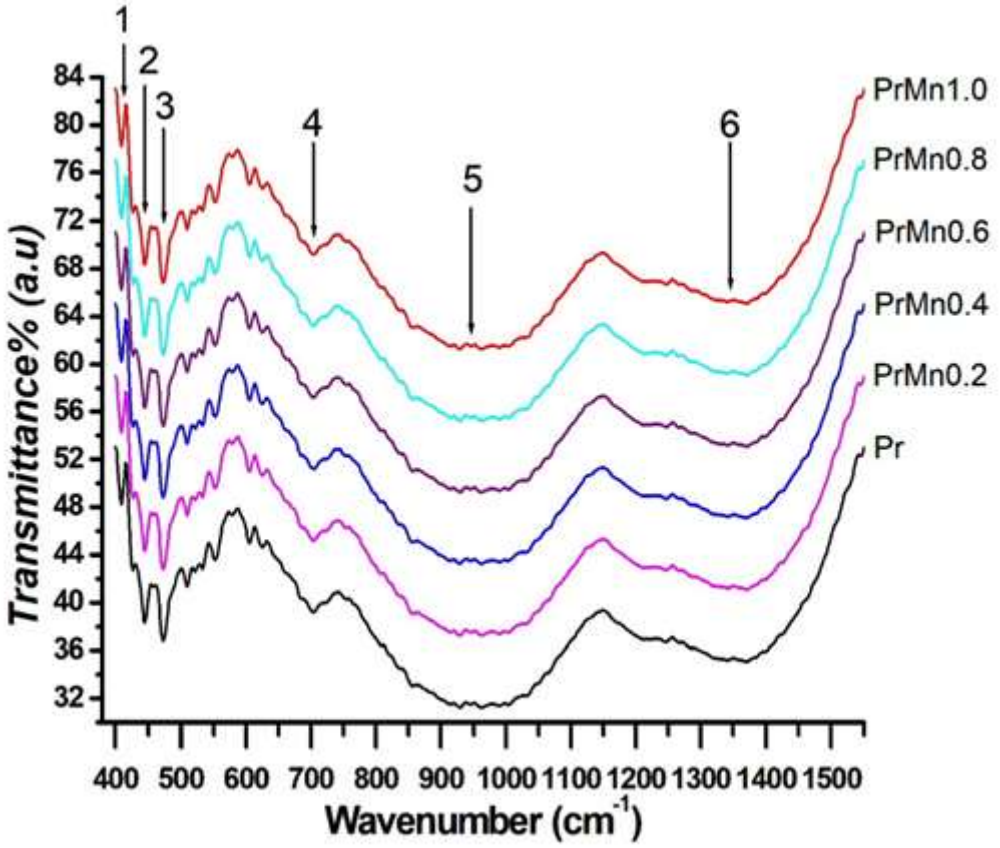


***Figure 6: FTIR spectra of CaO-PbO-$B_2O_3$-$SiO_2$ : $Pr^{3+}$- $Mn^{2+}$ ions co-doped glasses***

***Table 4: IR band positions CaO-PbO-$B_2O_3$-$SiO_2$ : $Pr^{3+}$ - $Mn^{2+}$ ions co-doped glasses***

| Band Position | Glass Samples | | | | | | Band Assignments |
|---|---|---|---|---|---|---|---|
| | Pr | PrMn0.2 | PrMn0.4 | PrMn0.6 | PrMn0.8 | PrMn1.0 | |
| 1 | 425 | 424 | 424 | 425 | 425 | 425 | Stretching and symmetrical bending vibrations of Pb–O in $PbO_4$ units |
| 2 | 456 | 455 | 456 | 455 | 456 | 456 | Combined Vibrations of $BO_3$ and $BO_4$ identities |
| 3 | 475 | 480 | 479 | 476 | 475 | 475 | Asymmetrical bending vibrations of Si–O–Si |
| 4 | 695 | 695 | 694 | 695 | 696 | 695 | Symmetrical bending vibrations of Si–O–Si |

ISSN: 2277-9655
Impact Factor: 5.164
CODEN: IJESS7

| | | | | | | | |
|---|---|---|---|---|---|---|---|
| 5 | 925 | 924 | 924 | 924 | 925 | 925 | Asymmetric vibration of B–O–Si units |
| 6 | 1390 | 1390 | 1392 | 1393 | 1390 | 1390 | Symmetric stretching relaxation of the B–O band of trigonal $BO_3$ units |

**4.6 Optical Absorption Spectra**

Optical Absorption Spectra is understanding sensitive tool to study the optical transitions and electronic band structure of RE ions and TM ions into co-doped glasses. The optical absorption spectra of CaO-PbO-$B_2O_3$-$SiO_2$ : $Pr^{3+}$- $Mn^{2+}$ ions co-doped glasses in the wavelength range between 200-2500 nm recorded at room temperature depicts in Figure 7. This absorption transition spectra of these glass samples exhibit eight absorption transitions corresponding to the $4f^2$-$4f^2$ intraconfigurational electric dipole transitions. All the transition in the absorption spectrum are started from the ground level ($^3H_4$) to various exited electronic levels $^3P_{2,\,1,\,0}$ , $^1D_2$, $^1G_4$, $^3F_{4,\,3,2}$ and $^3H_{6,5}$ are responsible for $Pr^{3+}$ species in the glass matrix [2, 3].

The established professional prominent sings of hump absorption transition of $Pr^{3+}$ ions: $^3H_4 \rightarrow {}^3P_2$ (at 448 nm), $^3H_4 \rightarrow {}^3P_1$ (at 469 nm), $^3H_4 \rightarrow {}^3P_0$ (at 485 nm), $^3H_4 \rightarrow {}^1D_2$ (at 590 nm), $^3H_4 \rightarrow {}^1G_4$ (at 1021 nm), $^3H_4 \rightarrow {}^3F_4$ (at 1433 nm), $^3H_4 \rightarrow {}^3F_3$ (at 1530 nm) and $^3H_4 \rightarrow {}^3F_2$ (at 1943 nm). From the observed absorption spectrograph, $^3H_4 \rightarrow {}^3P_{2,\,1,\,0}$ and $^1D_2$ are found in visible region and $^3H_4 \rightarrow {}^1G_4$ and $^3F_{4,\,3,\,2}$ are observed in the infrared region. M. Venkateswarlu, B. H. Rudramadevi and S. Buddhudu reported that, the optical absorption spectra of $Mn^{2+}$ doped glasses exhibited singe broad absorption transition at 456 nm corresponding to $^6A_{1g}$ ($^6S_{5/2}$) $\rightarrow {}^4T_{1g}$ ($^4G$) transition due to isolated $Mn^{2+}$ ions with octahedral symmetry [4-6].

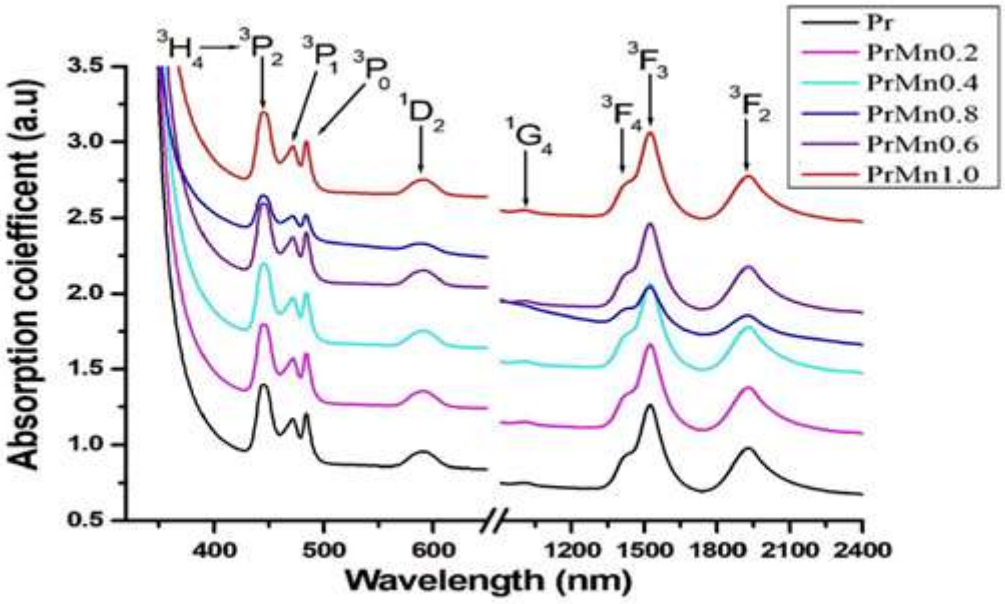


***Figure 7: Optical absorption spectra of CaO-PbO-$B_2O_3$-$SiO_2$: $Pr^{3+}$ - $Mn^{2+}$ co-doped glasses***

In the present work, we also recorded Uv-vis spectra of CaO-PbO-$B_2O_3$- $SiO_2$ glass system containing 1 mol% MnO content without $Pr_2O_3$ as display in Figure 8. It was observed from the Figure.8, 1 mol % of MnO content doped CaO-PbO-$B_2O_3$- $SiO_2$ glass exhibit a weak spin-forbidden absorption transition of $^6A_{1g}$ ($^6S$) $\rightarrow {}^4T_{1g}$ ($^4G$) at 448 nm indicates $Mn^{2+}$ ($d^5$) metal ions present in glass environment with octahedral cube geometry [7, 8].

ISSN: 2277-9655
Impact Factor: 5.164
CODEN: IJESS7

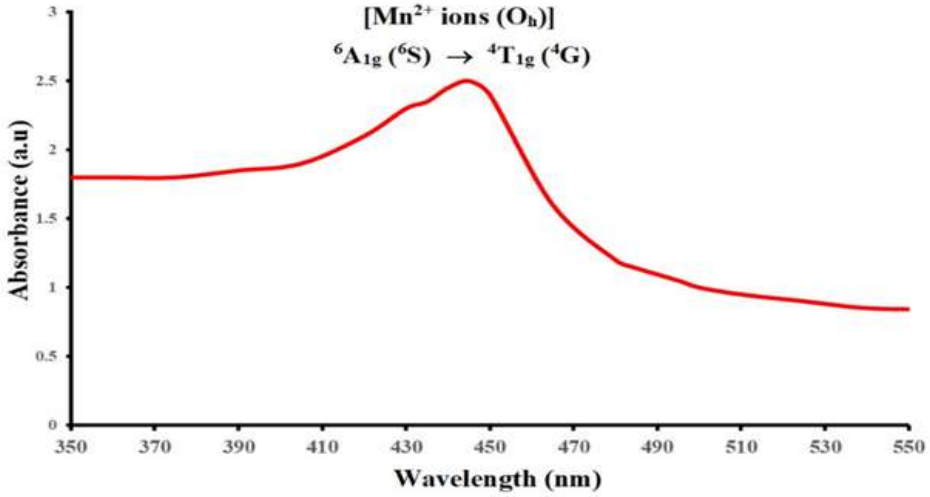


***Figure 8: Optical Absorption spectra of MnO doped CaO-PbO-$B_2O_3$-$SiO_2$ glass***

From the Figure.7 it was found that increasing mol% of MnO content in the present glass system, the $^6A_{1g}$ ($^6S$) $\rightarrow$ $^4T_{1g}$ ($^4G$) band is seems to be exactly merged with $^3H_4 \rightarrow {}^3P_2$ absorption band of $Pr^{3+}$ species.

**4.7 Electron Paramagnetic Resonance Spectra**

The EPR spectrogram of CaO-PbO-$B_2O_3$- $SiO_2$ : $Pr^{3+}$ - $Mn^{2+}$ pair of metal ions co-doped glasses were recorded at room temperature (35 $^oC$) shown in Figure.9. The EPR spectrogram was an sensitive analytical technical tool, it gives information about concerning valence state and local environment of paramagnetic identities of transition metal ions (TMI) in the glass environment. No ESR signal is observed in the ESR spectrogram of un-doped glass indicates that there is no paramagnetic metal ion identities. Due to presence of paramagnetic metal ions $Mn^{2+}$ ($d^5$) in the glass web and while increasing MnO mol % content, the sextet hyperfine structure (hfs) intensities were identified. The hfs line intensities were identified with increased with increment of MnO concentration. Additive of paramagnetic $Mn^{2+}$ ions, the glass samples exhibited two strong resonance intensity signals at g ≈ 2.00 and g ≈ 4.384. The hfs resonance signal at g ≈ 2.00 (centred and sextet signal) and additionally an intensive of sharp small hump signal at g ≈ 4.384 (157.5 mT) at left shoulder is due to isolated $Mn^{2+}$ ions predominantly located in octahedral lattice structure ($O_h$) [9, 10].

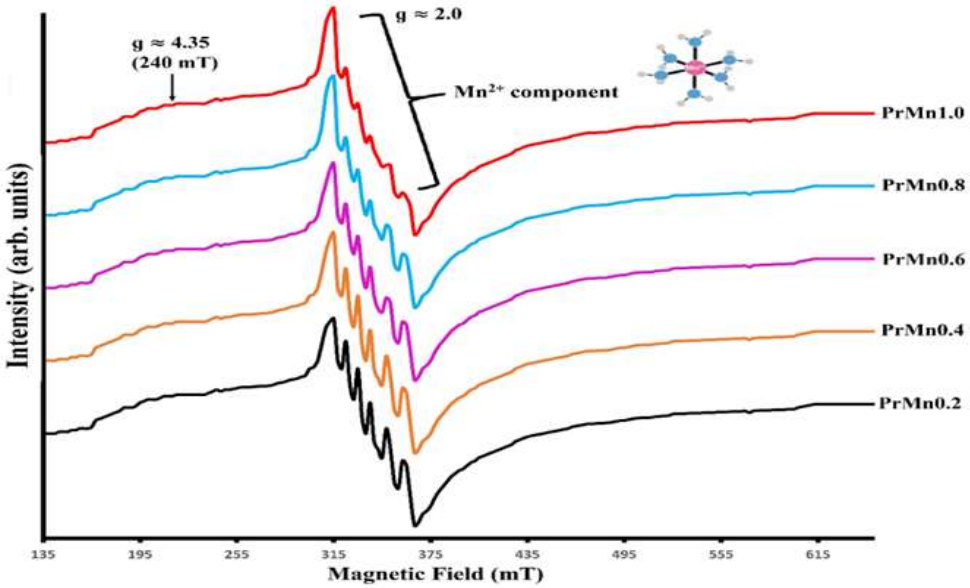


***Figure 9: EPR spectra of CaO-PbO-$B_2O_3$-$SiO_2$ : $Pr^{3+}$ - $Mn^{2+}$ co-doped glasses***

ISSN: 2277-9655
Impact Factor: 5.164
CODEN: IJESS7

**4.8 Photoluminescence Spectra (PL)**

The analysis of Photoluminescence Spectrogram determines, the two important experimental techniques to characterize luminescence transitions and energy transfer characteristics between Transition metal ion and Rare Earth ion of impurities in glass environment are absorption and excitation spectroscopy. The Figure.10 displays the photoluminescence spectra of $Pr^{3+}$ - $Mn^{2+}$ pair of metal ions co-doped CaO-PbO-$B_2O_3$- $SiO_2$ glasses. The luminescence spectra with an excitation wavelength ($\lambda_{exe}$) of 487 nm were recorded at room temperature. The PL spectra of CaO-PbO-$B_2O_3$- $SiO_2$ glasses containing $Pr^{3+}$ ions exhibits several emission transitions which are identified as $^3P_0 \rightarrow {}^3H_4$ (at 426 nm), $^3P_1 \rightarrow {}^3H_5$ (at 485 nm), $^3P_0 \rightarrow {}^3H_5$ (at 539 nm), $^1D_2 \rightarrow {}^3H_4$ (at 614 nm), $^3P_0 \rightarrow {}^3H_6$ (at 696 nm), $^3P_0 \rightarrow {}^3F_2$ (at 714 nm) and $^3P_1 \rightarrow {}^3F_3$ (at 752 nm) from the emission transition literature of $Pr^{3+}$ species [2, 3]. The co-doped Transition Metal ion and Rare Earth ion are serve as luminescence pair centers in inorganic oxide glasses. The $Mn^{2+}$ ion shows strong luminescence, the color of which can be changed over the range 490-750 nm depending on glass host materials [11, 12]. H. Chen and Y. Lei other researchers investigated and confirmed that the emission spectra of $Mn^{2+}$ ions exhibited a broad band of deep red peaked at 680 nm are observed, which comes from $^4T_{1g}$ ($^4G$) → $^6A_{1g}$ ($^6S$) spin-forbidden transition in the octahedral coordination sites [13]. While increasing strength of MnO in glass system the hyper sensitive emission transition is observed at 696 nm in PL emission spectra.

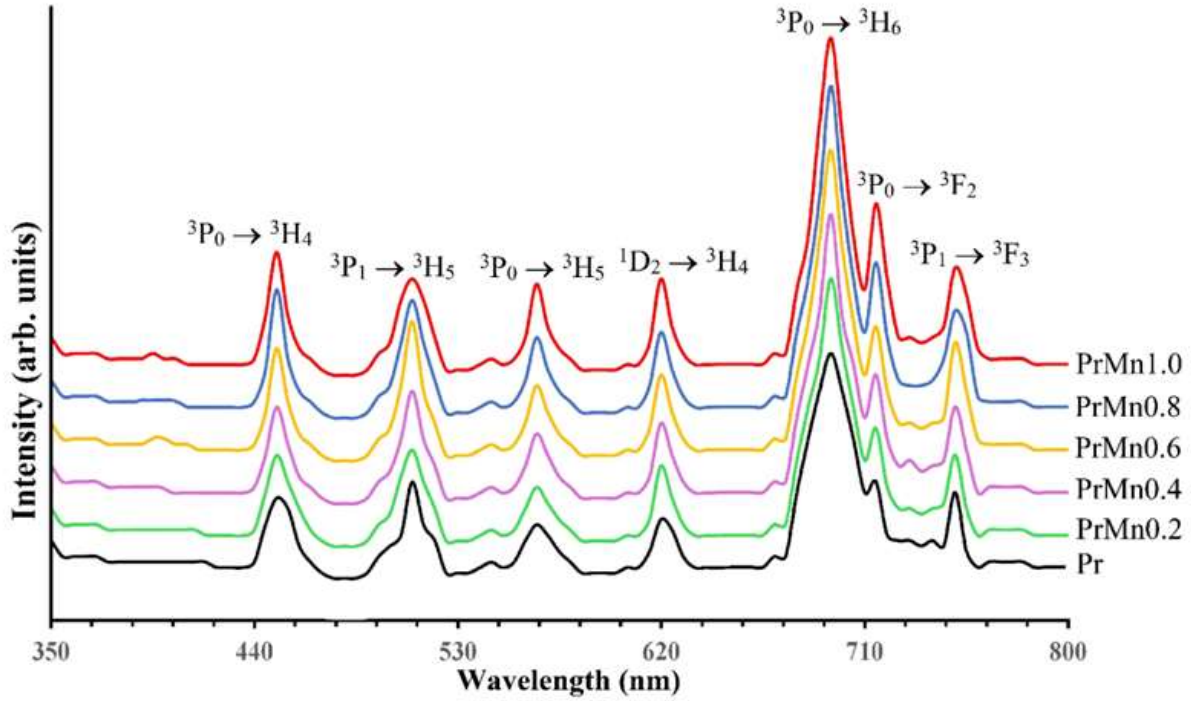


***Figure 10: PL spectra of CaO-PbO-$B_2O_3$-$SiO_2$ : $Pr^{3+}$ - $Mn^{2+}$ co-doped glasses***

## 5. DISCUSSION

Network glasses whose structure is liner and cross-linked give various linear polymeric changes are stacked over one another and liner polymeric chains are joined together to form a three dimensional glass network structures. The structure well and close packed in nature due to which they have high mechanical properties, hard nature, high densities, high melting point, high viscosity and high tensile strength. The spectroscopic properties of co-doped RE and TM ions in borosilicate glass host materials are subjected to rigorous interpretation that provides important contribution to contemporary scientific investigations. Among all oxide glasses, borosilicate glasses are good admixture of different impurities and three dimensional aspect spacious forming high stable network. Oxides of $SiO_2$ and $B_2O_3$ are strong glass forming reagents will form a strong and stable covalent bonds provides two dimensional network with oxygen anions.

ISSN: 2277-9655
Impact Factor: 5.164
CODEN: IJESS7

The fundamental unit in silicates is the silicon-oxygen tetrahedrons ($SiO_4$) which is composed of a central silicon ion ($\equiv Si^{4+}$-) surrounded by four closely packed and equally-spaced oxygen anions. The basic structural unit is [$SiO_4^{4-}$] and Si::O ratio is 1:4. The [$SiO_4^{4-}$] tetrahedron matrices with four surrounding oxygen atoms arranged to definite the corners of a tetrahedrons. When these [$SiO_4^{4-}$] tetrahedrons are linked together only corner oxygens will be shared with other [$SiO_4^{4-}$] groups. The bond ≡Si-O-Si≡ (in which one oxygen is shared between the two silicones is inert and strong linkage bond, $Si_2O_7^{4-}$). When each [$SiO_4^{4-}$] tetrahedrons is linked by sharing four of its corner oxygens to form infinite chain it is a single long chain $(Si_2O_6)^{4-}$. The Si-O bond mean distance is 0.016 Aº (0.16 nm) and Si-O band angle is 109º 47' and the chains consists of large number of tetrahedrons linked together. The bond angle between Si-O-Si structural link varies from 135º to 180º by differ of 4º-13º angle variation. The Si-O-Si bond dissociation energy 196 KJ/mol and Bond dissociate energy more for Si-O-Si self-linkage. The Self-linking property of Si atom and the rigid tetrahedral unit $[SiO_4]^{4-}$ forms three dimensional geometric network. Borosilicate structural units are packed together and coordinated by larger anions ($O^{2-}$) depends on the separation between cation and anion. The coordination number of ions mostly depended on ionic radius and relative size of ions. The CaO (Alkaline earth metal modifier) enters into the silicate network and depolymerizes to form meta, pyro and ortho silicates.

$$[\equiv Si\text{-}O\text{-}Si\equiv] + CaO \rightarrow [\equiv Si\text{-}O\text{-}Ca\text{-}O^-]$$

The additive of CaO (alkaline earth metal) partially stabilizes the $Si^{4+}$ with forming BO and NBO's. The $Ca^{2+}$ metal ions have fast ionic conducting nature in the glass environment to form more bonding defects with $CaO_6$ octahedral structural units. The $B_2O_3$ is the secondary glass network former in the borosilicate network glasses with 3-fold $[BO_{3/2}]^{3-}$ and 4-fold $[BO_{4/2}]^{4-}$ structural units. The addition of PbO (Heavy Metal Oxide modifier) enters into borosilicate glass web, which change the structural compactness, modifying local network connectivity and forming more interstitial defects and NBOs. The glass samples became highly stable against devitrification and chemical inert. At low mol % of PbO (> 50 mol %) act as glass modifier. In the 2D network borosilicate glass layout the silicate and borate structural units in the network strongly interact without PbO modifier with its structural unit $PbO_4$ dynamics creates more dangling bonds. In borosilicate glasses it is generally agreed that addition of modifier oxide PbO converted $[BO_3]$ to $[BO_4]$ units and form $PbB_4O_7$ complexes.

$$[BO_3]^{3-} + PbO \rightarrow [BO_4]^{4-} + Pb^{2+}$$
$$B_2O_3 + PbO \rightarrow PbB_4O_7$$

In the borosilicate network, the possible inter-tetrahedral avoidance that may exist between $[SiO_4]^{4-}$ and $[BO_4]^{4-}$ rigidity units in borosilicate glasses. The $[BO_4]^{4-}$ entities dominate in the silicate-rich domain, whereas $[BO_3]^{3-}$ boron entities prevail in the borate-rich hand and forms easily $\equiv B^{4+}\text{-}O^2\text{-}Si^{4+}\equiv$ (Borosilicate Bridge) linkage. In the borosilicate glass network, the silicate structural function groups dominate in coexistence of borate structural function groups. Each rigid $SiO_4$ tetrahedral structural unit linked with one $[SiO_4]^{4-}$ one $[BO_4]^4$ tetrahedral structural units and one oxygen from each unit linked with a metal ion and leads the structural formation of long 4-fold tetrahedral chains [14, 15]. Additions of modifiers into borosilicate glass system such as CaO, PbO, $Pr_2O_3$ and MnO, the 3D network is transferred to 2D network and finally settled in random network. Depolymerisation of glass network modifiers (CaO, PbO, $Pr_2O_3$ and MnO) in borosilicate glass host geometry take up the interstitial space between networking polyhedral, breaking up the periodicity of bonding oxygen and forming more NBO's in the glass environment.

The physical parameters and properties of all glass samples will play important vital key role in the quantitative determination of structural modification, structural compactness, NBOs, glass formers and modifiers, bonding parameters, transition metal ion strength, and alternation of cation-anion-action ions concentration. The density is the main function of physical properties of the glass sample to analyse the degree of structural compactness, connectivity, study the structural geometry of the glass and structural principal factors of glass composition. The refractive index of a glass sample is used to determine the suitability of glassy materials for optical band gap. The refractive index of the glass samples increasing trend indicating the decrement of interionic distance results the higher degree of disorder with in the glass network with increasing MnO content. The increasing Field strength of the glass samples were indicating increasing cross-linking packing and high degree of disorder. The increment of molar volume of glasses, revels the modification atomic geometrical configuration.

ISSN: 2277-9655
Impact Factor: 5.164
CODEN: IJESS7

The variation of quantities of density and molar volume of the glass samples in reverse trend indicating the increasing NBOs and cross-link density of the glass samples. The average molecular weight decreasing with increasing MnO content and retrospection of decrement of bonding oxygens (BO) and increment of NBOs in the glass density. The increasing trend of TM ion concentration in the glass network gives strong paramagnetic intensity of the ESR spectra analysis. The increasing Dielectric constant (ε) of all prepared glasses indicating increasing semiconducting property of glasses. Among all prepared glass samples the PrMn1.0 glass has highest value of optical basicity is observed and it was found that the optical basicity of the glass samples increasing trend with increment of mol % MnO dopant. The addition of $Pr^{3+}$ - $Mn^{2+}$ ions co-doped to the CaO-PbO-$B_2O_3$-$SiO_2$ glass web causes strongly influenced by the structural homogeneity, increase of NBOs, electron density carried by oxygen and increase degree of structural compactness of these prepared glasses with varying MnO content was observed from calculated physical parameters.

The melt-quenching process is a very simple technique for the preparation of the good transparent and high stable glasses. Glasses are disordered and cross-link structure and they don't have long range order. In the borosilicate glasses, the tetrahedral molecular dynamic structural units like $[SiO_4]^{4-}$ and $[BO_{4/2}]^{4-}$ are network connecting units. The borosilicate glasses have same type of arrangement of tetrahedral molecular dynamic structural units and it is arranged linearly like borosilicate molecular dynamic structural units. The tetrahedral molecular dynamic structural units of borosilicate structural units are joined together to form long straight chains like polymer molecular dynamic structural molecules. Borosilicate glasses contain arrangement of long, linear and cross-linked $[SiO_4]^{4-}$ and $[BO_{4/2}]^{4-}$ identical small borosilicate structural units to form borosilicate polymer glass network. The $BO_{4/2}$ units are interlocked with $SiO_{4/2}$ tetrahedrons. Borosilicate glass structure is like danburite structure. Addition of CaO, PbO, $Pr_2O_3$ and MnO into borosilicate layout, the linear ordered long chains are transformed to randomly and cross-linked network give well packed structure due to formation of more NBO's and more metal ion centres. With gradual increment of MnO mol% the IR Absorption line intensities are increased were observed in FTIR spectrogram.

The tetrahedral molecular dynamic structural units in borosilicate glasses which continually repeating the units in these glasses were observed from IR absorption spectra. The Borosilicate host glasses are considered to be remote composite glass composed of three network forming units namely $[SiO_4]^{4-}$, $[BO_{3/2}]^{3-}$ and $[BO_{4/2}]^{4-}$ molecular dynamic structural molecules in different proportions depending upon the glass remote composition. These molecular dynamic structural units forms covalent bonds to form more bridging oxygens in the glass network and instantly react with more electropositive elements like $Ca^{2+}$ and $Pb^{2+}$ to form NBOs in the glass network. The metal modifiers of CaO and PbO acts as stabilizers in the glass system.

The IR structural oscillator's spectra of CaO-PbO-$B_2O_3$-$SiO_2$: $Pr^{3+}$- $Mn^{2+}$ ions co-doped glasses exhibits various dynamic structural modes of bands with their structural oscillators. The first IR band ***($f_1$)*** at 425 $cm^{-1}$ attributed due to presence of Pb–O is weak definite band indication presence of $PbO_4$ structural units in the glass network [16, 17] and the stretching and symmetrical bending structural vibrations of $PbO_4$ units [18]**,** the second IR band ***($f_2$)*** at 456 $cm^{-1}$ attributed due to presence of Combined Vibrations of $BO_3$ and $BO_4$ structural oscillator, the third IR band ***($f_3$)*** at 475 $cm^{-1}$ attributed due to presences of Asymmetrical bending vibrations of ≡Si-O-Si≡ structural oscillator (Strong di-silicate linkage, $Si_2O_7$), the fourth IR band centered ***($f_4$)*** at 695 $cm^{-1}$ attributed due presence of Symmetrical bending vibrations of ≡Si-O-Si≡ structural oscillator (Strong di-silicate linkage, $Si_2O_7$), the fifth IR band ***($f_5$)*** at 925 $cm^{-1}$ attributed due presence of Asymmetric vibration of ≡B–O–Si≡ structural oscillator (Borosilicate linkage, weak Bridge) [19- 21] and the sixth IR band ***($f_6$)*** observed at 1390 $cm^{-1}$ Symmetric stretching relaxation of the B–O band of trigonal $BO_3$ structural oscillator [22].

The Borosilicate glass shows variable energy barrier order of breaking cation-oxygen-cation linkages strength sequence of ≡Si-O-Si≡ (very strong) > ≡B–O–Si≡ > ≡B-O-B= depend on additives of the network modifiers like CaO, PbO, MnO and $Pr_2O_3$. The mixing of the silicate and borate through sub-network formation of Si-O-B Bridge. The improvement of chemical flexibility, stability, cross linking strength of silicate glass by adding of Boron ($B^{4+}$) due to formation of relative, reliable and strong linkage of ≡$B^{4+}$-O-$Si^{4+}$≡ (Borosilicate linkage). The IR absorption spectrogram reveals the structural functional groups co-existence of borosilicate such as $[SiO_4]^{4-}$, $[BO_{3/2}]^{3-}$ and $[BO_{4/2}]^{4-}$ are identified in the glass network connectivity. In the glass environment, the Heavy metal Oxide (PbO) acts as glass modifier role in all prepared glass samples observed from FTIR spectra. The area of structural oscillators of IR bands increase with varying mol % of MnO additive. The gradual

ISSN: 2277-9655
Impact Factor: 5.164
CODEN: IJESS7

increase of mol% of MnO additive in sample glasses, the IR structural oscillator line intensities of the bands increase that indications of structural modifications and compactness of the glass layout. Manganese metal cations like $Ca^{2+}$ and $Pb^{2+}$ ions are expected to depolymerize in the glass network by producing more donor centres defects and NBO's**.** By increase mol % of MnO in the glass matrix, it was identified that the formation of large number of NBO's thus it indicates creation of more NBO's reduces the connectivity of the glass network. The isolated $Mn^{2+}$ metal cations are standard modifiers enters into the glass web occupies interstitial position like $Pb^{2+}$ cation. The isolated $Mn^{2+}$ ions octahedral cations ($O_h$) in the glass network the creation of more $V^{4+}$ donor centres is expected. The modifier and mobile ions present in glass web such as $Ca^{2+}$, $Pb^{2+}$, $Pr^{3+}$ and $Mn^{2+}$ are stabilize the charge in the glass environment. The modifier ions $Ca^{2+}$, $Pr^{3+}$ and $Mn^{2+}$ are occupies cubic geometry in the glass environment. The increasing degree of disorder in the glass web depends on the concentration and mol % of MnO. From IR spectra, it was observed that the $[SiO_4^{4-}]$, $[BO_4]^{4-}$ are tetrahedral groups (4-fold), $[BO_3]^{3-}$ (3-fold) and the oxygen was shared with octahedral cations such as $Ca^{2+}$, $Pb^{2+}$, $Pr^{3+}$ and $Mn^{2+}$ centres.

The study of optical absorption in the Uv-vis-NIR region is a useful sensitive technique to understand the electronic transition band and band structure between $Pr^{3+}$ and $Mn^{2+}$ ions co-doped $CaO\text{-}PbO\text{-}B_2O_3\text{-}SiO_2$ glasses. The $Pr^{3+}$ and $Mn^{2+}$ optical cations are easily distributed and randomly arranged into glass geometry. The Optical Absorption characterization of the glasses directly depends on its wavelength, affects colour of glass. The alteration of absorption transition wavelength reveals the colour. Rare earth elements mostly ionic form with trivalent state acts as charge stabilizers in the glass symmetry. The unique optical properties of lanthanide ions originate from electronic transitions with in the 4f sub-shell. The $Pr^{3+}$ metal optic centre exhibits eight absorption electronic band peaks which are attributed to the electronic transitions from the ground state ($^3H_4$) to different higher laying $4f^2$ states. Among various Rare earth metals the $Pr^{3+}$ metal ion exhibits activator role with electronic structure [Xe] $4f^2$ with a ground state ($^3H_4$) and excited state ($^3P_2$) which gives rise to various structured absorption transitions between wavelength ranges from 350 to 2500 nm. From the Optical Absorption spectrogram it was observed that the Optical line intensities are increasing trend upto 0.6 mol% decrease to 0.8% and increase upto 1.0 mol% doped by MnO due to its high compactness glass structure, increasing local cross-link density and structural modification. The average Pr-O distance is to decrease in the glass geometry, this influence acquiring of hypertensive electronic absorption transition of $^3H_4 \rightarrow {}^3P_2$ and comparing others the average Pr-O distance maybe increased. Among all the absorption transitions, a significant $^3H_4 \rightarrow {}^3P_2$ is observed as hypersensitive with highest intense. Among 3d transition metal period, the $Mn^{2+}$ ion has a ground state ($^6A_{1g}$) [spherically non-degenerate] in octahedral symmetry, which is lowest according to Hund's rule. In glasses, the Manganese in $Mn^{2+}$ ($3d^5$) ion with half-filled stable configuration with free-ion terms $^6S$, $^4G$, $^4D$ and $^4F$. The optical spectra have been analysed in the frame-work of crystal field theory [23, 24]. The excited quartet states $^4G$, $^4P$, $^4D$ and $^4F$ of $Mn^{2+}$ ions in the octahedral (cubic) crystal field are situated above the ground $^6S$ state. Hence all the transitions from the ground sextet $^6S$ to the excited energy levels (spin quartet or doublet) are spin-forbidden and the intensity of optical absorption lines of $Mn^{2+}$ are weak. Transition metal ions ($Mn^{2+}$) exhibits colour due to the presence of unpaired electrons 3d sub-shell which undergo d-d transition. The $Mn^{2+}$ ions has a ground state ($^6A_{1g}$) [spherically non-degenerate] with octahedral symmetry and excited state ($^4T_{1g}$). The $Mn^{2+}$ optical metal centres gives only one weak spin-forbidden transition assigned as [$^6A_{1g}$ ($^6S_{5/2}$) $\rightarrow$ $^4T_{1g}$ ($^4G$)] weak intense depends on crystal field parameter (Dq) in the glass matrix at 448 nm (UV-vis region) due its stable half-filled electronic configuration ($3d^5$) [25-27].

From the optical absorption spectra figures 7 & 8, the significant strong absorption transition merged between the $Mn^{2+}$: $^6A_{1g}$ ($^6S_{5/2}$) $\rightarrow$ $^4T_{1g}$ ($^4G$) and the $Pr^{3+}$: $^3H_4 \rightarrow {}^3P_2$ electronic bands. From the observed absorption edges, we have evaluated the optical band gaps ($E_o$) of these glasses by drawing Tauc plots between $(\alpha h\nu)^{1/2}$ and $h\nu$ as per the following equation

$$\alpha(\nu)\, h\nu = C\,(h\nu - E_o)^n \qquad \ldots\ldots\ldots (1)$$

Here the exponent (n) can take values 1/2 and 2 for indirect, direct transitions and C is a constant in glasses respectively [28]. Tauc plots for direct transition are shown in Figure.11 (a) and indirect transitions are shown in Figure 11 (b). Extrapolating the linear portion of these plots as $(\alpha h\nu)^{1/2} = 0$, $(\alpha h\nu)^2 = 0$ gives optical band gap, the theoretical band gap energy is calculated using the equation $E=hc/\lambda$. Urbach Energy ($\Delta E$) was evaluated from the slopes of the linear regions of the curves and taking their reciprocals. Urbach Energy ($\Delta E$) that indicates a

ISSN: 2277-9655
Impact Factor: 5.164
CODEN: IJESS7

measure of a disorder in glassy environment are shown in Figure 12. The cut-off wavelength ($\lambda_c$), direct and indirect band energy gaps and Urbach Energy ($\Delta E$) data is given in Table 5.

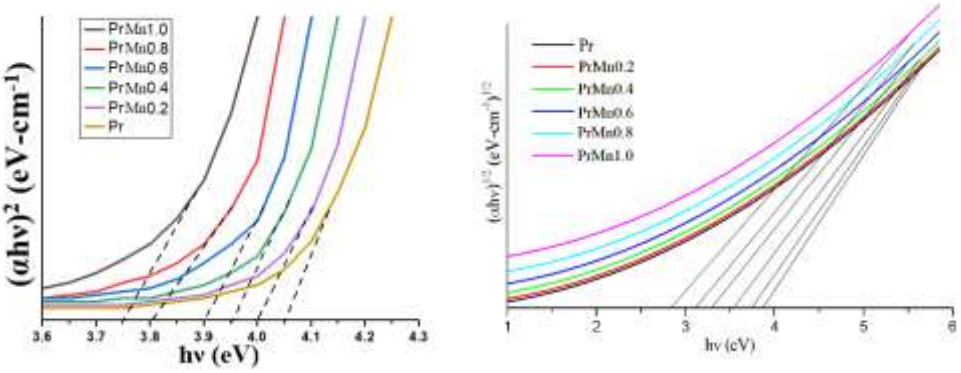


***Figure 11 (a) & 11 (b): Tauc plots to evaluate (a) direct band gap (b) In-direct band gap of CaO-PbO-$B_2O_3$-$SiO_2$: $Pr^{3+}$- $Mn^{2+}$ ions co-doped glasses***

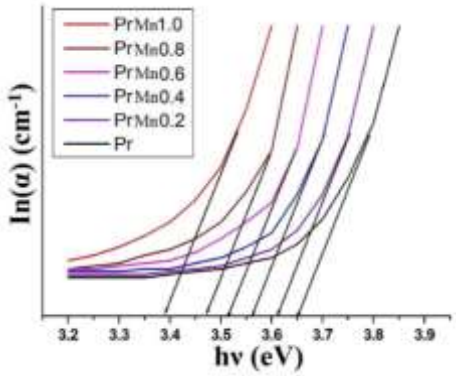


***Figure 12: A plots of In(α) and hv for CaO-PbO-$B_2O_3$-$SiO_2$: $Pr^{3+}$- $Mn^{2+}$ ions co-doped glasses***

***Table 5: The cut-off wavelength ($\lambda_c$), Optical band gaps ($E_g$) and Urbach energy of CaO-PbO-$B_2O_3$-$SiO_2$: $Pr^{3+}$ - $Mn^{2+}$ ions co-doped glasses***

| Glass Sample | Cut-off wavelength $\lambda_C$ (nm) | Theoretical Band gap (eV) | Direct Band gap (eV) | Indirect Band gap (eV) | Urbach energy (ΔE) (eV) |
|---|---|---|---|---|---|
| Pr | 354 | 3.8671 | 4.0576 | 3.9911 | 0.2754 |
| PrMn0.2 | 357 | 3.8116 | 4.0033 | 3.7912 | 0.2879 |
| PrMn0.4 | 363 | 3.7214 | 3.9441 | 3.5544 | 0.3116 |
| PrMn0.6 | 365 | 3.5516 | 3.9026 | 3.3785 | 0.3346 |
| PrMn0.8 | 368 | 3.3106 | 3.8119 | 3.2191 | 0.3457 |
| PrMn1.0 | 372 | 3.1032 | 3.7567 | 2.9767 | 0.3625 |

From the Table.5 It was observed that direct and indirect optical band gaps energy decreasing trend while increasing mol% of MnO additive. The cut-off wavelength ($\lambda_c$) of all prepared glass samples were shifted towards higher wavelength region in absorption spectra and at the same instant Urbach Energy ($\Delta E$) values increasing trend with introduction of MnO was observed from Table 5. The Urbach energy ($\Delta E$) of glass

ISSN: 2277-9655
Impact Factor: 5.164
CODEN: IJESS7

samples to determine the structural local disorders and with the localized states in glassy geometry. The Urbach energy (ΔE) values are observed to be increasing trend with RI and increase of $Mn^{2+}$ ion concentration, this indicating the increasing of local structural disorder, structural modification, cross linking density and decrease of network connectivity.

The addition of Manganese in various glass matrices its oxidation states in the glass environment depending on the quantitative properties of glass formers and modifiers, size of the anions and cations in the glass geometry, their crystal field parameters, strength of crystal field mobility of the modifier cations and concentration of MnO content. While increasing specific volume of glasses indicates that $Pr^{3+}$ ion are substituted in $Ca^{2+}$ ion sites [29, 30] [$Pr^{3+}$ -1.12 A$^o$] [$Ca^{2+}$ -1.13 A$^o$]. The $Pr^{3+}$ ion has very similar ionic radii with $Ca^{2+}$ ion but more of the electronic charge of the cloud and $Pr^{3+}$ metal centre may exhibit different site distribution characteristics instead of $Ca^{2+}$ ion. Moreover increasing molar volume of glass samples, due to the favourable isovalent replacement of $Pb^{2+}$ by $Mn^{2+}$ metal ions. The $Pr^{3+}$ ($4f^2$) ion exhibits 91 micro-states. The isolated $Pr^{3+}$ metal ions enters at higher concentration (1 mol %) into the glass network as a modifier and isolated $Pr^{3+}$ ions occupy intestinal positions with 6-fold coordination sites in the glass environment [31, 32]. Moreover the optical absorption spectral studies indicate the Mn ions are predominantly in the $Mn^{2+}$ stable valence state and adopt modifier octahedral cube positons.

The lowest optical band gap of PrMn1.0 glass sample was observed due to increasing of cross-link strength, induced disorders, static disorders, glass structural disorder, imperfection, increase of NBO's and decreasing connectivity increasing MnO additive. The increasing the Urbach energy (ΔE) evaluations the glass samples are indicating increasing semiconductor nature. The isolated $Mn^{2+}$ cations obviously present in these prepared glasses and occupy interstitial positions like $Pr^{3+}$ simple ion.

A convenient standard method representing the intensity of an absorption band is to measure the oscillator strength of the transition which is observed to be proportional to the area under the absorption line shapes. The quantitatively comprehend Optical phenomena of rare earth ions in glasses, it is of great importance to evaluate radiative and non-radiative decay process of related 4f levels. The Judd-Ofelt theory is usually adopted to obtain the transition probabilities including radiative decay rate by utilizing the data of absorption cross sections of several f-f electric-dipole transitions. From the optical absorption spectra, the calculated and experimental oscillator strengths of the absorption transitions are estimated in terms of the area under an absorption peak.

$$f_{exp} = 4.318\text{x}10^{-9} \int \varepsilon(\nu) d\nu \ \text{dv} \qquad \text{---------- (2)}$$

Where ε (ν) denotes the molar extinction coefficient at a wave number ν in $cm^{-1}$.

According to the J-O theory [33, 34] the oscillator strength of electric-dipole *f-f* transition of trivalent rare earth ions from a level *(ψJ)* to a particular final state *(ψ′J′)* is given as

$$f(\psi J; \psi' J') = \frac{\upsilon}{(2j+1)} \left[\frac{8\pi^2 mc(n^2+2)^2}{3h(9n)}\right] \sum_{\lambda=2,4,6} \Omega_\lambda \langle (\psi_J \| U^\lambda \| \psi'_{J'})^2 \rangle \qquad \text{------- (3)}$$

where 'm' refer to the mass of the electron, 'c' is the velocity of light in vacuum, 'h' is the plank's constant, *J* and *J′* are the total angular moment of the initial and final levels, n is the refractive index of refraction of the glass, $\Omega_\lambda$ (λ=2, 4, 6) are the material parameters and $\|U_\lambda\|^2$ are the doubly reduced matrix elements of the unit tensor operator of the rank λ=2, 4 and 6. The rms deviations between the experimental and calculated energy value are very small, indicating the validity of the full matrix diagonalization.

$$\delta_{rms} = \sqrt{\left[\frac{\Sigma(f_{exp} - f_{cal})^2}{N}\right]} \qquad \text{------- (4)}$$

Where N is the total number of transitions involved in the fitting

Applied standard J-O intensity parameters $\Omega_\lambda$ (λ=2, 4, 6) are evaluated from the least square fitting procedure using experimentally measured oscillator strength for $Pr^{3+}$ - $Mn^{2+}$ ions co-doped CaO-PbO-$B_2O_3$-$SiO_2$

ISSN: 2277-9655
Impact Factor: 5.164
CODEN: IJESS7

glasses. The calculated experimental standard oscillator strengths ***($f_{exp}$)*** and standard oscillator strengths ***($f_{cal}$)*** the obtained values are given in Table 6. The Applied standard J-O intensity parameters determined in the present glass network are observed to be in the trend $\Omega_4 > \Omega_6 > \Omega_2$ as shown in Table 7.

***Table 6: Theoretical and experimental oscillator strength of CaO-PbO-$B_2O_3$-$SiO_2$: $Pr^{3+}$ - $Mn^{2+}$ ions co-doped glasses***

| Transition from $^3H_4$ | GLASS SAMPLES | | | | | | | | | | | |
|---|---|---|---|---|---|---|---|---|---|---|---|---|
| | Pr | | PrMn0.2 | | PrMn0.4 | | PrMn0.6 | | PrMn0.8 | | PrMn1.0 | |
| | $f_{cal}$ ($x10^{-6}$) | $f_{exp}$ ($x10^{-6}$) | $f_{cal}$ ($x10^{-6}$) | $f_{exp}$ ($x10^{-6}$) | $f_{cal}$ ($x10^{-6}$) | $f_{exp}$ ($x10^{-6}$) | $f_{cal}$ ($x10^{-6}$) | $f_{exp}$ ($x10^{-6}$) | $f_{cal}$ ($x10^{-6}$) | $f_{exp}$ ($x10^{-6}$) | $f_{cal}$ ($x10^{-6}$) | $f_{exp}$ ($x10^{-6}$) |
| $^3P_2$ | 5.6805 | 5.6876 | 5.6914 | 5.6897 | 5.6787 | 5.6753 | 5.6716 | 5.6691 | 5.6657 | 5.6604 | 5.6556 | 5.6481 |
| $^3P_1$ | 2.1814 | 2.1829 | 2.1915 | 2.1993 | 2.1855 | 2.1846 | 2.1797 | 2.1759 | 2.1677 | 2.1664 | 2.1523 | 2.1494 |
| $^3P_0$ | 3.6818 | 3.6678 | 3.7114 | 3.7009 | 3.6891 | 3.6844 | 3.6006 | 3.5904 | 3.5454 | 3.5414 | 3.5119 | 3.4919 |
| $^1D_2$ | 1.5997 | 1.5944 | 1.6712 | 1.6674 | 1.5886 | 1.5817 | 1.4911 | 1.4901 | 1.4833 | 1.4821 | 1.4791 | 1.4711 |
| $^1G_4$ | 0.3756 | 0.3755 | 0.3861 | 0.3814 | 0.3788 | 0.3756 | 0.3718 | 3.6876 | 3.6759 | 3.6678 | 3.6117 | 3.6019 |
| $^3F_4$ | 3.8711 | 3.8701 | 3.8999 | 3.8978 | 3.8813 | 3.5794 | 3.7104 | 3.7009 | 3.6717 | 3.6693 | 3.6114 | 3.6001 |
| $^3F_3$ | 4.4619 | 4.4574 | 4.5019 | 4.4994 | 4.4326 | 4.4276 | 4.3117 | 4.3089 | 4.2719 | 4.2691 | 2.2515 | 2.2478 |
| $^3F_2$ | 2.3184 | 2.3047 | 2.3661 | 2.3603 | 2.2676 | 2.2577 | 2.2341 | 2.2304 | 2.2811 | 2.2714 | 2.2.69 | 2.2008 |
| Rms deviation | 0.0449 | | 0.0614 | | 0.0476 | | 0.0486 | | 0.0498 | | 0.0421 | |

***Table 7: J-O Parameters of CaO-PbO-$B_2O_3$-$SiO_2$: $Pr^{3+}$ - $Mn^{2+}$ ions co-doped glasses***

| Glasses Samples | $\Omega_2 x10^{-20}$ ($cm^{-2}$) | $\Omega_4 x10^{-20}$ ($cm^{-2}$) | $\Omega_6 x10^{-20}$ ($cm^{-2}$) | Trend |
|---|---|---|---|---|
| Pr | 1.26 | 5.79 | 3.98 | $\Omega_4 > \Omega_6 > \Omega_2$ |
| PrMn0.2 | 1.29 | 5.61 | 3.94 | $\Omega_4 > \Omega_6 > \Omega_2$ |
| PrMn0.4 | 1.21 | 5.54 | 3.87 | $\Omega_4 > \Omega_6 > \Omega_2$ |
| PrMn0.6 | 1.15 | 5.47 | 3.81 | $\Omega_4 > \Omega_6 > \Omega_2$ |
| PrMn0.8 | 1.09 | 5.38 | 3.78 | $\Omega_4 > \Omega_6 > \Omega_2$ |
| PrMn1.0 | 1.05 | 5.33 | 4.01 | $\Omega_4 > \Omega_6 > \Omega_2$ |

The $\Omega_2$ parameter strongly depends on the short range effects, such as covalency of the $Pr^{3+}$ ion and sensitive to the symmetry of $Pr^{3+}$ ion site, while $\Omega_4$ and $\Omega_6$ are long-range parameters related to the bulk properties of the glass such as rigidity and viscosity [35]. The optical absorption spectrogram of $Pr^{3+}$ - $Mn^{2+}$ pair of metal ions in CaO-PbO-$B_2O_3$-$SiO_2$ glass web was influenced the structure of the glass geometry when the $Pr^{3+}$ and $Mn^{2+}$ ions are incorporated into glasses. From the Figure.7 and Table.7, the $^3H_4 \rightarrow {}^3P_2$ hypertensive transition observed from optical absorption spectra of $Pr^{3+}$ and standard J-O intensity analysis. The $Pr^{3+}$ and $Mn^{2+}$ both metal ions in these glass systems are representative network modifier positions their relevant octahedral positions.

Electron Paramagnetic resonance (EPR) spectroscopy is one of the most sensitive methods such as hyperfine structure, perturbations and consequently it has been widely used to detect and characterize paramagnetic

ISSN: 2277-9655
Impact Factor: 5.164
CODEN: IJESS7

entities in glasses. This method was successfully applied to elucidate the oxidation state, the symmetry and type of the coordination sites of various Transition metal ions complexed in glasses. Each electron in an atom or ion behaves like a tiny magnet. Its magnetic moment originates from two types of motions (i) its orbital motion around the nucleus and (ii) its spin around its own axis. Only the TM ions influence the EPR spectrum due to ideal presence of $Mn^{2+}$ paramagnetic ions. The different oxidation states shown by Manganese are: +2 (MnO, $MnCO_3$, $MnCl_2$), +3 ($Mn_2O_3$, $MnF_3$), +4 ($MnO_2$), +5 ($K_3MnO_4$), +6 ($K_2MnO_4$), +7 ($KMnO_4$, $Mn_2O_7$). The oxidation states of an element depends on its electronic configuration and the number of unpaired electrons. Among Manganese oxidation states, $Mn^{2+}$ and $Mn^{7+}$ are most stable oxidation states.

The $Mn^{2+}$ (II) is most stable because it has the half-filled configuration [Ar] $3d^5$. When the transition metal ions are coordinated with other glass matrix ions, the energy levels of the 3d electrons are split by the electric filed of the coordinated ions. The d-electron orbitals are strongly directional, so the splitting is sensitive to the arrangement of the surrounding ions. Thus transition metal ions are used to probe the glass structure and to study the coordination number of central ions due to their outer d-electron orbital functions have a broad radial distribution. Although among Manganese oxidation states and covalence, +2 is most stable oxidation valence due to its half-filled electronic configuration i.e. five single electrons present in d-orbital having same $m_s$ value (+1/2). Since the total spin of $3d^5$ orbital is $\pm 5/2$ due to this $Mn^{2+}$ ions exhibits strong field splitting which is sensitive to the local environment. Glass is diamagnetic nature of web. The paramagnetic $Mn^{2+}$ entities are introduced in the diamagnetic glass web, the induce of paramagnetic nature in glass environment and glass lattice structure this affects generation of $Mn^{2+}$ ($^6S_{5/2}$, $3d^5$) sextet hyperfine resonance increasing peak areas are observed in the EPR spectrogram.

The EPR intensity signal amplitudes are increasing trend with increasing mol% of MnO additive. The paramagnetic spectrogram of $Mn^{2+}$ paramagnetic metal ions shows lines indicating group of small peaks in the external applied magnetic field resembles isolated fine structures. The EPR signal in the central range and the simultaneous appearance of relatively sextet peaks suggest the presence parameter of $Mn^{2+}$ (II) ion. The second one is that sextet lines appear which arises from interactions between electron spin and nuclear spin in Manganese ions which is also called hyperfine interactions. The sextet signal centred at $g_{eff}$ = 2.00 is a finger-point of paramagnetic $Mn^{2+}$ ions subject to hyperfine magnetic interaction with I = 5/2 spin $^{55}Mn$ nucleus [36].

The average hyperfine splitting between neighbouring peaks of the $Mn^{2+}$ sextet reflects, approximately, the degree of iconicity of the bonds involving the Manganese ion (II). The EPR constitutes of $Mn^{2+}$ paramagnetic centres are in octahedral cubic symmetry site [37, 38]. From the Figure.9, the resonance signal at g= 2.0 exhibit due to $Mn^{2+}$ paramagnetic ion in glass environment occupies the octahedral symmetry [39- 41] and participated dipole – dipole interaction or super exchange interactions may be arises of $Mn^{2+}$ paramagnetic ions. While the intensity of broad resonance at g=4.384 (157.5 mT) increased with increase of MnO content. The board resonance at g=4.384 (157.5 mT) exhibit due to spin-spin interactions of $Mn^{2+}$-$Mn^{2+}$ paramagnetic ions. The hyperfine magnetic interactions are responsible for the magnetic splitting of typical $Mn^{2+}$ EPR signal on account of their common high spin $3d^5$ (L=0) electronic state because $Mn^{2+}$ ion have anisotropy energy [42]. The EPR spectrogram of all glass samples exhibits strong predominant signals at g=2.0 (with sextet hyperfine structure) and g=4.384 (left shoulder) presence of $Mn^{2+}$ paramagnetic ion. The well-resolved strong hyperfine splitting resonance signals is due to $Mn^{2+}$ paramagnetic metal ion occupy its octahedral symmetry.

A novel pair of RE ion ($Pr^{3+}$) and Transition metal ion ($Mn^{2+}$) were co-doped into CaO-PbO-$B_2O_3$-$SiO_2$ glasses. The TM and RE ions exist in different oxidation states ($Mn^{2+}$, $Pr^{3+}$) in the prepared glasses. Rare earth ions have important characteristics which distinguish them from other optically active ions: they emit and absorb over wavelength ranges due to its more metastable states. The isolated $Pr^{3+}$ ion, as well-known activator role dopant possess unique optical and luminescence properties along with the tuneable emission wavelengths ranging from orange to red visible colour regions. Rare-earth elements are important optical activators for luminescent devices. Among various rare-earth luminescent centers, trivalent praseodymium ($Pr^{3+}$) offers simultaneously a strong emission in the blue, green, orange, and red spectral range, satisfying the complementary color relationship [43, 44]

Moreover, new optical characteristics are expected in the $Mn^{2+}$ and $Pr^{3+}$ ions co-doped glass system, for example strong luminescence due to both $Mn^{2+}$ and $Pr^{3+}$ ions co-doped was observed in CaO-PbO-$B_2O_3$-$SiO_2$

ISSN: 2277-9655
Impact Factor: 5.164
CODEN: IJESS7

glass web. Efficient sensitizer - acceptor ions energy transfer give strong luminescence visible color. The isolated $Mn^{2+}$ ions could exhibit a varying broad band emission from green to deep red depending its host lattice. The $Mn^{2+}$ ions in a weak crystal filed can emit green light, while $Mn^{2+}$ ions in a strong crystal field would give rise to a red. Borosilicate glass system doped with $Mn^{2+}$ ion have exhibited a broad emission band ranging from 550 to 725 nm which is determined by the matrix crystal field. Red emission is demonstrated in strong crystal fields of octahedral coordinated sites [45 - 47]. The luminescent isolated $Mn^{2+}$ ion exhibits variable colours form green → yellow → red in depending on the remote glass composition. Whereas octahedral coordinated $Mn^{2+}$ ion (stronger crystal field) results in orange to red emission [48]. The increasing MnO concentration the emission shifts towards higher wavelength region (red colour) present in octahedral symmetry interaction of strong crystal field (CF). The MnO additive is energy sensitizer to $Pr^{3+}$ Activator ions [49].

The energy levels of the $3d^5$ state depend strongly on the crystal field. Excitation into the higher d-states relaxes non-radiatively to the first excited state ($^4T_{1g}$) with subsequent broad emission to the ground state ($^6A_1$). Thus the inter-ionic energy transfer between rare earth ions and $Mn^{2+}$ is a prospective possibility. The transition metal $Mn^{2+}$ can provide a broad emission band in the visible range corresponding to d-d transition and its emission varies from green to deep red depending on the crystal field since the emission efficiency of d-d transition due to spin electric dipole transitions sensitizing $Mn^{2+}$ ions [50]. The divalent Manganese ($Mn^{2+}$) is a considered as a sensitizer efficient energy for almost all trivalent rare earth ions [51]. The red shift was already indicative that the increase of manganese concentration increasing the crystal field strength [51]. Due to the non-radiative energy transfer from $Mn^{2+}$ to $Pr^{3+}$ rare earth ion, luminescent intensity and hence the optical gain of the transitions can be enhanced. The red luminescent $Mn^{2+}$ ions of $^4T_{1g}$ ($^4G$) → $^6A_{1g}$ ($^6S$) transition is the source of this signal and octahedrally coordinated ions [52 - 55].

Upon exciting at 487 nm, the emission spectra monitoring of $Mn^{2+}$ and $Pr^{3+}$ ions, these are several emission bands located in the spectral range 400 to 800 nm. In PL spectra of $Mn^{2+}$ ion exhibit strong emission transition due to its strong crystal field strength. All emission transitions of $Pr^{3+}$ ion are assigned of the 4f-4f interaconfigurational transitions. The emission transition of $Pr^{3+}$ ion for the principle inter manifold transitions from $^3P_{1,\ 0}$ and $^1D_2$ energy states to the lower laying manifolds in the visible region. From the luminescence spectra, the significant strong spectral binding between the $Mn^{2+}$ : [$3d^5$, $^4T_{1g}$ ($^4G$) → $^6A_{1g}$ ($^6S_{5/2}$)] and the $Pr^{3+}$: [$4f^2$, $^3P_0$ → $^3H_6$] provides strong resonant energy transfer transition from $Mn^{2+}$ ion (sensitizer) to $Pr^{3+}$ ion (activator). The high intensity luminescence transition characterizes the lasing power of the glass among various transitions. Among all the emission transitions the luminescent hyper transitions of $^3P_0$ → $^3H_6$ is conceded as Red laser transition. The emission intensity of transitions mainly originates from the manifolds of $^3P_{0,1}$ states increases proportional to the $Pr^{3+}$ and $Mn^{2+}$ ions concentrations upto 1 mol%. In this present paper study, $Mn^{2+}$: [$3d^5$, $^4T_{1g}$ ($^4G$) → $^6A_{1g}$ ($^6S_{5/2}$)] (donor) strong crystal field energy is transferred to $Pr^{3+}$: [$4f^2$, $^3P_0$ → $^3H_6$] (acceptor) and this is represented in the simplified energy level diagram of $Mn^{2+}$ → $Pr^{3+}$ ions in Figure: 13.

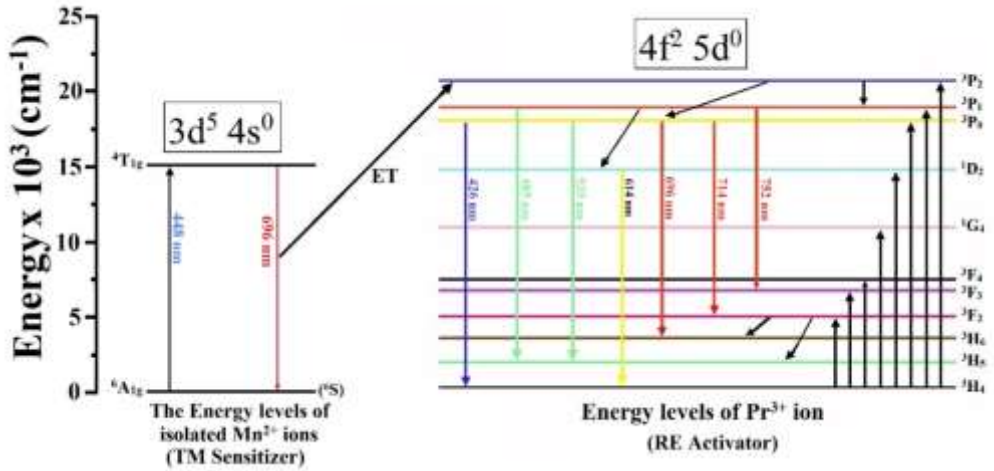


***Figure 13: Simplified Energy level diagram of CaO-PbO-$B_2O_3$-$SiO_2$: $Pr^{3+}$ - $Mn^{2+}$ ions co-doped glasses***

ISSN: 2277-9655
Impact Factor: 5.164
CODEN: IJESS7

The first theoretical formulation of pair transfer that successfully identifies the inverse sixth power distance dependence was made by Förester [56]. From the Förester pair transfer theory, the donor (Sensitizer) – acceptor (Activator) separations $R_o$ (Förester distance - critical separation distance – mean distance) substantially smaller than the wavelengths of visible radiation and Förester energy transfer is the short-range asymptote. By use of the Fermi rule [57], the rate of energy transfer between a Sensitizer and Activator pair has a quadratic dependence on the quantum amplitude. The Förester parameter ($R_o$) that characterizes the strength of the dipole-dipole contribution to the energy transfer probability. According to T. Förester - D. L. Dexter theory the change of Non-radiative energy transfer from $Mn^{2+} \rightarrow Pr^{3+}$ through multipole interaction is immerse. Specially, the RE and TM pair of doped ions has consideration of turned to glass systems in which each Sensitizer and Activator pair has optical and emission properties that satisfy the spectral electronic transition binding condition. Substantial, the spectral overlap between donor and acceptor orbitals is therefore a prerequisite for rapid exchange energy transfer. The spectral electronic transition spatial merged requirements to limit the exchange mechanism to short-range [Förester parameter ($R_o$)] energy transfers between closely situated chromophores and includes all intramolecular electrostatic interactions. The transfer efficiency is also dependent on the type of interaction and the distance of $Mn^{2+} \rightarrow Pr^{3+}$ ions. Due to larger crystal field is expected in $Mn^{2+} \rightarrow Pr^{3+}$ ions in glass environment resulting bright red emission towards higher wavelength is observed at high concentration of co-dopants.

The energy transfer process, the interionic separation (R) is the main parameter controlling the energy transfer process. As the concentration of the activator ions increase, the Förester distance ($R_o$) between $Pr^{3+}$ and $Mn^{2+}$ ions was given below linear equation

$$R = \sqrt[3]{\left(\frac{3V}{4\pi N}\right)} \qquad \text{-------- (5)}$$

Where V is the volume of the lattice, C is the sum of $Pr^{3+}$ and $Mn^{2+}$ concentrations

While the highest co-dopant mol % of $Pr^{3+}$ and $Mn^{2+}$ ions are used in this present paper, the Förester distance was calculated by given above linear equation the value of $R_o$ (Förester distance) ≈ 16.2 A°. In glass geometry, due to strong crystal field strength of $Mn^{2+}$ ions and less mean distance ($R_o$) between donor ($Mn^{2+}$) and acceptor ($Pr^{3+}$) gives results strong, high intense emission of higher wavelength region. As well as for the Förester distance ($R_o$) associated decrease of $Pr^{3+}$ - $Mn^{2+}$ pair distance due to the spatial separation for strong luminescent emission of bright red colour. Among all PL emissions, $^3P_0 \rightarrow {}^3H_6$ is hyper intensity transitions observed and the intensity of $^3P_0 \rightarrow {}^3H_6$ transition is increased with increasing pair dopants of Pr and Mn mol %. The Bright Red emission is observed in the $Mn^{2+}$ ion was doped into the glass CaO-PbO-$B_2O_3$-$SiO_2$ : $Pr^{3+}$ which is ascribed to the $^4T_{1g}$ ($^4G$) $\rightarrow$ $^6A_{1g}$ ($^6S$) transition of the $Mn^{2+}$ ions. Moreover the $Mn^{2+}$ emission bands depending on the surroundings of host, size of $Mn^{2+}$ion, size of $Pr^{3+}$ ions and Förester distance between $Pr^{3+}$ - $Mn^{2+}$ ions. From the energy level diagram between $Pr^{3+}$-$Mn^{2+}$ revels that $Mn^{2+}$ ion is a high stable versatile sensitizer for $Pr^{3+}$ activator ion of Bright Red emitter.

From the J-O theory radiative results shows that the energy transfer from $Mn^{2+}$ ions (emission) to $Pr^{3+}$ ions (absorption) in the co-doped CaO-PbO-$B_2O_3$-$SiO_2$ glass system as shown in Table.8, which converts emission of $Mn^{2+}$ (696 nm, $^4T_{1g} \rightarrow {}^6A_{1g}$) ion into bright red emission of $Pr^{3+}$ (696 nm, $^3P_0 \rightarrow {}^3H_6$). This implies that the co-doped samples, the emission of $Mn^{2+}$ ion is the direct reabsorption by $Pr^{3+}$ ion itself [$Mn^{2+}$ ($d^5$)$\rightarrow$ $Pr^{3+}$ ($f^2$)]. The bright red emission from the highest f-sub shell laying state ($^3P_0$) to lower levels. The radiative properties of $Pr^{3+}$ ions in the glass web depends on the number of factors such as network formers, modifiers, intermediates, replacement of one metal ion by another metal ions, concentration and mol % of $Pr^{3+}$ ions, nature of bonding, spectroscopic parameters, concentration and mol % of $Mn^{2+}$ and finally critical distance between $Pr^{3+}$ and $Mn^{2+}$ pair of ions.

***Table 8: Various radiative properties of CaO-PbO-$B_2O_3$-$SiO_2$: $Pr^{3+}$ - $Mn^{2+}$ ions co-doped glasses***

| | GLASS SAMPLES | | | | | |
|---|---|---|---|---|---|---|
| Transitions | Pr | PrMn0.2 | PrMn0.4 | PrMn0.6 | PrMn0.8 | PrMn1.0 |

ISSN: 2277-9655
Impact Factor: 5.164
CODEN: IJESS7

| | A($s^{-1}$) | β% | A($s^{-1}$) | β% | A($s^{-1}$) | β% | A($s^{-1}$) | β% | A($s^{-1}$) | β% | A($s^{-1}$) | β% |
|---|---|---|---|---|---|---|---|---|---|---|---|---|
| $^3P_0 \rightarrow {}^3H_4$ | 1542 | 13.49 | 1619 | 2.98 | 1590 | 13.78 | 1581 | 14.89 | 1561 | 13.41 | 1486 | 13.01 |
| $^3P_1 \rightarrow {}^3H_5$ | 942 | 11.77 | 1077 | 11.88 | 1066 | 11.78 | 1006 | 11.55 | 989 | 11.46 | 978 | 11.21 |
| $^3P_0 \rightarrow {}^3H_5$ | 1486 | 13.44 | 1579 | 2.87 | 1556 | 13.97 | 1534 | 14.49 | 1521 | 13.78 | 1511 | 13.64 |
| $^1D_2 \rightarrow {}^3H_4$ | 669 | 6.91 | 719 | 7.42 | 714 | 7.36 | 692 | 7.18 | 682 | 6.96 | 678 | 6.85 |
| $^3P_0 \rightarrow {}^3H_6$ | 3217 | 42.39 | 3446 | 47.87 | 3372 | 47.21 | 3305 | 46.67 | 3275 | 46.19 | 3233 | 45.86 |
| $^3P_0 \rightarrow {}^3F_2$ | 2758 | 33.44 | 2880 | 34.42 | 2864 | 34.31 | 2839 | 34.19 | 2806 | 33.91 | 2779 | 33.63 |
| $^3P_1 \rightarrow {}^3F_3$ | 2236 | 15.16 | 2326 | 16.89 | 2313 | 16.72 | 2286 | 16.56 | 2272 | 16.17 | 2251 | 16.02 |
| $A_T$ ($s^{-1}$) | 7656.63 | | 8347.86 | | 7446.56 | | 7355.66 | | 6916.76 | | 7114.21 | |

From the observed all emission transitions originated mostly from the $^3P_0$ populated energy level. The non-radiative transition probability was found to increasing in the emission levels order of $^3P_0 > {}^3P_1 > {}^1D_2$ in prepared sample glasses. Here $^3P_{2,\,1,\,0}$ and $^1D_2$ are most populated energy states of $Pr^{3+}$ ions for emission of visible color (Blue, Green, Yellow or Red). The energy transfer transition mechanism of luminescence spectra, after excitation of $Pr^{3+}$ ions to $^3P_2$ states, non-radiative de-excitation occurred from $^3P_2$ to $^3P_1$, $^3P_0$ and $^1D_2$ states. Finally, the photon emission takes place from $^3P_1$, $^3P_0$ and $^1D_2$ states to lower lying levels. The Population on $^3P_0$ state of $Pr^{3+}$ ions in NR (non-radiative) and glass was achieved by multi-phonon assistance process. Where population on $^3P_0$ state can be directly achieved. Such as when $^3P_0$ state is populated, transition from $^3P_0$ too many other lower energy levels $^3H_5$, $^3H_6$, $^3F_2$ manifolds is observed. The emission intensity of transitions mainly ordinates from the manifolds of $^3P_{0,\,1}$ shells increase proportional to the $Pr^{3+}$ and $Mn^{2+}$ ions concentrations 0 to 1 mol%. Resonance energy transfer usually occurs in the ultraviolet or visible range of the electromagnetic spectrum, which is comparable to the energy required for electronic transitions between sensitizer and activator. In the energy transfer transition (ETT) process of Non-radiative multiphoton relaxation process, the excitation absorption energy of the $Pr^{3+}$ ion was transformed into a discrete number of phonons. The Non-radiative resonant energy transfer process may be either an exchange interaction or multipole-multipole interaction we assume the interaction is of the electric dipole-dipole quadrupole type. According to Dexter- Förester, the non-radiative energy Transfer (ET) between Mn ions can take place by radiative reabsorption by excitation energy, exchange interaction or multipolar interaction. The activator of $Pr^{3+}$ ion have various meta-stable energy levels ($^3P_{2,\,1,\,0}$ $^1D_2$) from which appreciable for non-radiative emission transitions. Among $^3P_0 \rightarrow {}^3H_6$ show strong radiative red laser tendency. The ET occur between a pair of dissimilar luminescent centres or between identical luminescent centres. The case of dissimilar luminescent centres involves to centres: a sensitizer ($Mn^{2+}$) and an activator ($Pr^{3+}$). The Addition of Ca (alkali earth metal) modifier to the glass matrix can increase intensity of luminescence emission of glass [58] and other modifier additive of PbO (Heavy metal oxide) possess high chemical stability, high refractive indices and spontaneous strong emission probabilities [59, 60]. The addition of $Pr^{3+}$ and $Mn^{2+}$ cations acts as inducers of charge balancers in the entire glass geometric network.

From the Figure.13, the Energy Transfer Mechanism (ETM) between $Mn^{2+}$ and $Pr^{3+}$ ions is evidence of energy transfer of [$Mn^{2+}$: $^4T_{1g}$ ($^4G$) $\rightarrow$ $^6A_{1g}$ ($^6S_{5/2}$) ] $\rightarrow$ [$Pr^{3+}$ : $^3P_0 \rightarrow {}^3H_6$] transition were observed in $Mn^{2+} \rightarrow Pr^{3+}$: CaO – PbO – $B_2O_3$- $SiO_2$ co-doped glasses. The enhanced bright red emission (696 nm) of the $Mn^{2+}$ ions due to an ideal effective energy transfer from $Mn^{2+}$ (Sensitizer) to $Pr^{3+}$ (activator) ions in the CaO-PbO-$B_2O_3$-$SiO_2$ glass. The standard J-O comparison of "β" for all glass samples, suggests good value for the glass PrMn1.0. From this observations suggests that, 1.0 mol% of MnO is more optimal high concentration in this glass geometry to produce high luminescence efficiency of red emission. The energy level of $Pr^{3+}$ close to the $Mn^{2+}$ emitting state, this indicates that possibility of energy transfer takes place from divalent manganese to trivalent praseodymium ion ($d^5 \rightarrow f^2$ sub-shells). Which turns increases the energy transfer as is clear in the glass PrMn1.0 composition.

The CIE chromaticity coordinates for all co-doped glass samples are calculated and results are listed in Table.9 and depicts in Figure: 14.

ISSN: 2277-9655
Impact Factor: 5.164
CODEN: IJESS7

***Table 9: The color coordinates of CaO-PbO-$B_2O_3$-$SiO_2$: $Pr^{3+}$ - $Mn^{2+}$ ions co-doped glasses***

| Glasses Samples | X | Y |
|---|---|---|
| Pr | 0.63055 | 0.31079 |
| PrMn0.2 | 0.64237 | 0.30796 |
| PrMn0.4 | 0.64748 | 0.30112 |
| PrMn0.6 | 0.65545 | 0.29297 |
| PrMn0.8 | 0.65687 | 0.28115 |
| PrMn1.0 | 0.66833 | 0.27006 |

The emitting color of the glasses is in red with increasing mol% of MnO additive. Particularly the CIE chromaticity coordinates for PrMn1.0 is in bright red color. This glass can be recommended as a good glass web that can emit red laser. From this reason, CaO-PbO-$B_2O_3$-$SiO_2$: $Pr^{3+}$ - $Mn^{2+}$ ions co-doped glasses have high potential applications in the field of optical fibers, red color light sensors, LED displays and optical applications.

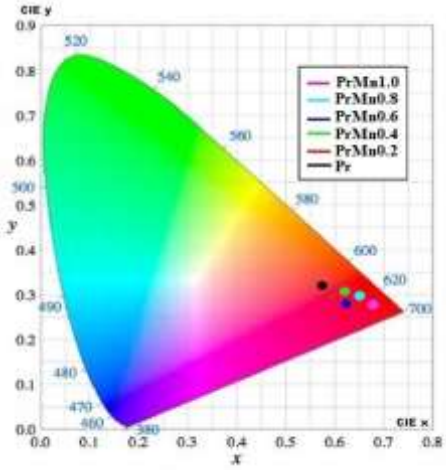


***Figure 14: The color space chromaticity diagram of CaO-PbO-$B_2O_3$-$SiO_2$ : $Pr^{3+}$ - $Mn^{2+}$ co-doped glasses***

## 6. CONCLUSION

The novel synthesis of remote glass composition web of CaO-PbO-$B_2O_3$-$SiO_2$ were co-doped with $Pr^{3+}$ - $Mn^{2+}$ ions by melt-quenching process. These glass samples were characterized and analyzed by XRD, DTA, FTIR, Optical Absorption, EPR and Photoluminescence spectra. The main conclusion of this present paper studies are as follows:

1. The oxidation state of Pr and Mn co-doped metal ions and their geometric coordination in the CaO-PbO-$B_2O_3$-$SiO_2$ glasses have been investigated by using spectroscopic analysis.
2. Various physical parameters of glass samples are calculated from linear equations. The important physical parameters glasses such as density, average molecular weight, refractive index, interionic distances, TM ion concentrations, optical dielectric constant and dielectric constant are studied in the present work.
3. The results of XRD spectra, it is clear the glass formation was confirmed and co-doped all glassy samples were in Non-crystalline structure without any sharp Bragg's peaks. From the EDS reviewed results, all the participating elements are forming stable and high quality structural homogeneity glasses.
4. The DTA spectrograph reflects the network modifiers are strongly influence the $T_g$ and modification of chemical boding parameters between the glass modifiers and formers. Moreover, the temperature gradually increasing upto $T_g$ in the oxide glass increasing chemical bond strength (between cation-anion-cation), Strong closeness packing, chemical durability and cross-linking density. From DTA

ISSN: 2277-9655
Impact Factor: 5.164
CODEN: IJESS7

spectrogram results of all the glasses reveal PrV1.0 glass is highly stable against devitrification increasing MnO concentration.

5. The IR spectral studies of these glass samples exhibited Borosilicate fundamental structural oscillator absorption bands ($SiO_4$, $BO_3$ and $BO_4$) are observed. With increase in MnO additive concentration shows the increasing intensity of IR lines indicates Borosilicate structural homogeneity, structural alternation and increasing borosilicate connectivity in the glass network. The structural dynamic variations of all prepared glass samples were analysed and studied by IR absorption spectra.
6. Tracing the resonance $Mn^{2+}$ ion magnetic field values as a function of field orientations. Tracing the resonance of $Mn^{2+}$ ions hyperfine structure with sextet magnetic interactions of paramagnetic ions. The investigated all samples from the EPR measurement exhibits strong resonance signals which are characteristic of the $Mn^{2+}$ paramagnetic ions. The paramagnetic $Mn^{2+}$ resonance signal at g= 2.02 shows a six line hyperfine structure due to the $Mn^{2+}$ ions are in octahedral symmetry. In addition a prominent peak with at g= 4.35 left shoulder was observed.
7. The Optical absorption analysis exhibits that a notable single exactly merged transition of $Mn^{2+}$ [$^6A_{1g}$ ($^6S_{5/2}$) → $^4T_{1g}$ ($^4G$)] and $Pr^{3+}$ [$^3H_4$ → $^3P_2$] ions. The optical absorption parameters like cut-off wavelength ($\lambda_c$), direct and indirect band gaps energy values are calculated all glasses. The lower value of optical band gap of PrMn1.0 indicates higher degrees of disorder and structural defects in this glass.
8. The $Pr^{3+}$ ions exhibits in several absorption and emission transitions in the contained glass network. In the present paper study, the Optical absorption spectra and Luminescence spectra were characterized by applied J-O statistics.
9. From the PL spectrogram results of CaO-PbO-$B_2O_3$-$SiO_2$ : $Pr^{3+}$ - $Mn^{2+}$ ions co-doped glass system, it is observed that a notable $^3P_0 \rightarrow {}^3H_6$ significant transition fall in bright red region at 696 nm due to energy transfer from $^4T_{1g}$ ($^4G$) → $^6A_{1g}$ ($^6S_{5/2}$) transition of $Mn^{2+}$ ions to $^3P_0 \rightarrow {}^3H_6$ level of $Pr^{3+}$ ions. The sensitized $Mn^{2+}$ luminescence has been realized based on the $Mn^{2+} \rightarrow Pr^{3+}$ Energy transfer transition was observed in the CaO-PbO-$B_2O_3$-$SiO_2$ : $Pr^{3+}$ - $Mn^{2+}$ ions co-doped glass system.
10. The notable binding the energy transfer transition from $Mn^{2+}$ ion of [$^4T_{1g} \rightarrow {}^4A_{1g}$] (sensitizer, donor, emission) to $Pr^{3+}$ ion (activator, acceptor, absorber) resulting in the characteristic Bright Red emission of $^3P_0 \rightarrow {}^3H_6$ hyper transition from $Pr^{3+}$ ions. From PL spectra and the J-O theory statistics results show that the efficient $Mn^{2+} \rightarrow Pr^{3+}$ Energy transfer transition probability maximum for glass sample PrMn1.0.
11. From the Optical Absorption spectra and Photoluminescence spectra results $Mn^{2+}$ and $Pr^{3+}$ ions occupy higher coordination of octahedral ($O_h$) symmetry of co-doped glass samples.
12. CaO-PbO-$B_2O_3$-$SiO_2$ : $Pr^{3+}$ - $Mn^{2+}$ ions co-doped glass system analysis of the spectroscopic studies of $3d^5 \rightarrow 4f^2$ transfer of electron (Isolated energy transfer of $d^5 \rightarrow f^2$ ) which are great interest for application in laser and attain high luminescent efficiency.
13. The isolated $d^5 \rightarrow f^2$ charge transfer is type of metal to metal intervalence charge transfer state revels of the d → f transition of $Mn^{2+} \rightarrow Pr^{3+}$ ions co-doped CaO-PbO-$B_2O_3$-$SiO_2$ glass system.
14. The CIE chromaticity coordinates, it was identified that PrMn1.0 glass fall in bright red. The PrMn1.0 sample can be used as Red laser emitting semiconductor materials. The PrMn1.0 glass have wide range potential technological applications in optical components, optoelectronic devices, optic communication, color glass filters, memory devices and sensors.

## REFERENCES

[1]Vishal kumar. O.P. Pandey, K. Singh, Physica B 405 (2010) 204.

[2] Danilo Manzani, David Paboeuf, Philippe Goldner, Fabien Bretenaker, Opt. Mater. 35(2013) 383–386.

[3] P. Vijaya Lakshmi, T. Sambasiva Rao, K. Neeraja, D.V. Krishna Reddy, N. Veeraiah, M. Rami Reddy,

Journal of Luminescence 190 (2017) 379–385.

[4] M. Venkateswarlu, B. H. Rudramadevi and S. Buddhudu, IOSR-JAP e-ISSN: 2278-4861. Volume 7,

Issue 4 Ver. III (2015), PP 05-12.

[5] A. Murali, R.P. Sreekanth Chakradhar, J. Lakshmana Rao, Physica B 358 (2005) 19-26.

ISSN: 2277-9655
Impact Factor: 5.164
CODEN: IJESS7

[6] R.P. Sreekanth Chakradhar, K.P. Ramesh, J.L. Rao, J. Ramakrishan, J Phys Chem Solids, Volume 64, Issue 4 (2003), Pages 641-650. https://doi.org/10.1016/S0022-3697(02)00365-7

[7] Shiv Prakash Singh, R.P.S Chakradhar, J.L, Rao, Basudeb Karmakar, Physica B 405 (2010) 2157- 161.

[8] D.K. Durga, N. Veeraiah, J Phys Chem Solids. 64 (2003) 133-146.

[9] Li L L, Wu S Y and Kaung M Q 2011 Spectrochim. Acta A 79 82.

[10] Krishna R M et al 1999 Mater. Res, Bull. 34 1521.

[11] Hernandex JA, Camarillo EG, Munoz G, Flores CJ, Cabreara EB, Jaque F, Romeo JJ, Sole JG, Murrieta HS (2001) Opt Mater 17:491.

[12] Wang XJ, Jia D, Yen WM (2003) J Lumin 102-103:34.

[13] H. Chen, Y. Lei, J.aaQA Li, K. Chen, L. Wu, L. Zheng, T. Sun, Y. Kong, Y. Zhang and J. Xu, Inorg. Chem, 2022, 61, 5495-5501.

[14] R. P. Sreekanth Chandradhar, B. Yasoda, J.L. Rao, J. Non-Cryst. Solids 353 (2007) 2355-2362.

[15] G. Naga Raju, M. Srinivasa Reddy, K.S.V Sudhakar, N. Veeraish, Opt. Mater. 29 (2007) 1467-1474.

[16] Subbalakshmi P & Veeraiah N, Phys Chem Glassses 45(2001) 307.

[17] Nageswara Rao K & Veeraiah N, Indian J Phys, 74A (2000) 37.

[18] M.S. Gaafar, S.Y. Marzouk, I.S. Mahmoud, Results in Physics, 22 (2021) 103944.

[19] T.G.V.M. Rao, A. Rupesh Kumar, K. Neeraja, N. Veeraiah, M. Rami Reddy, J. Alloy. Compd. 557(2013) 209-217.

[20] Y. Lai, Y. Zeng, X. Tang, H. Zhang, Z. Han, H. Su, RSC Adv. 6 (96) (2016) 93722-97728.

[21] C. Gautam, A.K. Yadav, V. K. Mishra, K. Vikram, 2 (4) (2012) 47-54.

[22] J. Zhong, X. Ma, H. Lu, X. Wang, S. Zhang, W. Xiang, J. Alloy. Compd. 607 (2014) 177-182.

[23] Sviridov D.T., Sviridova R.L. and Smirnov Yu.F. Optical spectra of transition metal ions in crystals, Nauka, Moscow, 1976 (in Russian)

[24] Henderson B. and Bartram R.H. Crystal-field engineering of solid-state laser materials, Cambridge University Press, Cambridge, 2000.

[25] K. Vijaya Babu, A. Subba Rao, K. Naresh Kumar and M. Venugopala Rao, Journal of Aircraft and Spacecraft Technology, (2019) Volume 3: 248-255.

[26] Yu-Sheng Dou, Equations for calculating Dq and B, J. Chem. Edu. 67 (1990) 134.

[27] H. Togashi, N. Kojima, T. Ban, I. Tsujikawa, Bull. Chem. Soc. Jpn. 61 (1998) 1903.

[28] Davis, E. A., Philos. mag. 22 (1970) 903-922.

[29] Milojkov, D.V; Silvestre, O.F; Stanic, V.D.; Janic, G.V.: Mutavdzic, D.R.; Milanovic, M.; Nieder, J.B.

ISSN: 2277-9655
Impact Factor: 5.164
CODEN: IJESS7

Fabrication and characterization of luminescent Pr3+ doped fluorapatitie nanocrystals as bioimaging contrast agents. J. Lumin. 2020, 217, 116757.

[30] Fleet, M.E.; Pan, Y. Site preference of rare earth elements in fluorapatite. Am. Mineral. 1995, 80, 329-335.

[31] Shelby J E 1994 Key Eng. Mater. 94 43.

[32] Zhou XJ, Tanner PA, Faucher MD, (2007) Luminescence of CS2NaScCl6:Pr3+: effects of changing the lattice parameter. Sectro Lett 40: 349-366.

[33] Judd BR, Phys Rev. 127:750-761 (1962).

[34] Ofelt GS, J Chem Phys 37:511-520 (1962)

[35] Srinivastave P, Rai SB, Rai DK. J Alloys Compd 368:1-7 (2004).

[36] Van Wieringen, J.S. Paramagnetic Resonance of Divalent Manganese Incorporated in Various Lattice. Discuss. Faraday Soc. 1955, 19,118-126.

[37] Li L L, Wu S Y and Kaung M Q 2011 Spectrochim. Acta A 79 82.

[38] Krishna R M et al 1999 Mater. Res. Bull. 34 1521.

[39] Giridhar G, Rangacharyulu M, Ravikumar R V S S N and Sambasiva Rao P, 2009 IOP Conf. Ser.: Mater. Sci. Eng. 2 012058.

[40] Hirokazu Masai, Yusuke Hino, Takayuki Yanagida, Yutaka Fujimoto, Opt. Mater. 42 (2015) 381-384.

[41] V. Volpi, M. Montesso, S. J. L. Ribeiro, W.R. Viali, C. J. Magon, I.D.A. Silva, J.P. Donoso, M. Nalin, J. Non-cryst. Solids 431 (2016) 135-139.

[42] Mantel, C.; Philouze, C.; Collomb, M.N.; Duboc, C. Eur. J. Inorg. Chem. 2004, 3880-3886.

[43] Birkhahn R, Garter M, Steckl AJ: Red light emission by photoluminescence and electroluminescence from Pr-doped GaN on Si substrates. Appl Phys Lett 1999, 74:2161.

[44] Wang W, Jiang C, Shen MR, Fang L, Zheng FG, Wu XL, Shen JC: Effect of oxygen vacancies on the red emission of SrTiO3:Pr3+phosphor films. Appl Phys Lett 2009, 94:081904.

[45] Pasinski, D.; Sokolnicki, J. Broadband orange phosphor by energy transfer between Ce3+ and Mn2+ in Ca3Al2Ge3O12 garnet host. J. Alloys Compd. 2019, 786, 808-816.

[46] Dong, R.; Liu, W.; Song, Y.; Zhang, X.; An, Z.; Zhou, X.; Zheng, K.; Sheng, Y.; Shi, Z.; Zou, H. A promising single-phase, color-tunable phosphor (Ba0.9Sr0.1)9 Lu2Si6O24: Eu2+, Mn2+ phosphors for near-ultraviolet white-light-emitting diodes. J. Lumin. 2019, 214, 116585.

[47]Yan, J.; Zhang, Z.; Wen, D.; Zhou, J.; Xu, Y.; LI, J.; Ma, C-G.; Shi, J,; Wu, M. Crystal structure and

ISSN: 2277-9655
Impact Factor: 5.164
CODEN: IJESS7

photoluminescence tuning of novel single-phase Ca8ZnLu(PO4)7 Eu2+, Mn2+ Phosphors for near-UV converted white light-emitting diodes. J. Mater. Chem. C 2019, 7, 8374-8382.

[48] Gao, G.; Reibstein, S.; Peng, M.; Wondraczek, L. Dual-mode photoluminescence from Mn2+ doped Li, Zn aluminosilicate glass ceramics. Physics and Chemistry of Glasses: European Journal of Glass Science and Technology, Part B 2011, 52(2), 59-63.

[49] B.C. Joshi, M.C. Joshi, B.D. Joshi, J. Phys. Chem. Solids 52 (1991) 939.

[50] H. Zeng, Q. Yu and Z. Wang, J. Am. Ceram. Soc., 2013, 96, 2476-2480.

[51] R. Reisfeld, M. Eyal, C. Jacoboni, Chem. Phys. Lett. 129 (1986) 292.

[52] Kemeny G, Haake CH (1960) J Chem Phys 33:783

[53] Bingharam K, Parke S (1965) Phys Chem Glasses 6:224

[54] Menassa PE, Simkin DJ, Taylor P (1986) J Lumin 35:223

[55] Tanaka M, Qi J, Masumoto Y (2000) J Lumin 87-89:472

[56] T. Förester, "Zwischenmolekulare Energiewanderung und Fluoreszenz", Annalen. Phys. 2, 55-75 (1978).

[57] E. Fermi, Nuclear Physics, University of Chicago press, Chicago (1950).

[58] Kaewkhao J., Wantana N., Kaewjang S., Kothan S., Kim H.J. (2016). Luminescence characteristic of Dy3+ doped Gd2O3-CaO-SiO2-B2O3 scintillating glasses, J. Rare Earth. 34: 583-589.

[59] W.H. Dumbaugh, J.C. Lapp. J. Am. Ceram. Soc. 75 (1998) 169.

[60] L.C. Courrol, L.R.P. Kassab, V.D.D. Cacho, S.H. Tatumi, N.V. Wetter, J. Lumin. 102 (2003) 101.